

Forced vibration of surface foundation on multi-layered half space

Lin Chen*

*Lehrstuhl für Baustatik und Baudynamik, RWTH Aachen University,
Mies-van-der-Rohe-Str. 1, 52074 Aachen, Germany*

(Received April 2, 2014, Revised October 15, 2014, Accepted November 6, 2014)

Abstract. A numerical approach is presented for the analysis of the forced vibration of a rigid surface foundation with arbitrary shape. In the analysis, the foundation is discretized into a number of sub square-elements. The dynamic response within each sub-element is described by the Green's function, which is obtained by the Fourier-Bessel transform and Precise Integration Method (PIM). Incorporating the displacement boundary condition and force equilibrium of the foundation, it obtains a system of linear algebraic equation in terms of the contact forces within each sub-element. Solving the equation leads to the desired dynamic impedance functions of the foundation. Numerical results are obtained for foundation not only with simple geometrical configurations, such as rectangular and circular foundation, but also the case of irregularly shaped foundation. Several comparisons between the proposed approach and other methods are made. Very good agreement is reached. Also, parametric studies are carried out on the dynamic response of foundation. Addressed in this study are the effects of Poisson's ratio, material damping and contact condition of soil-foundation interface. Several conclusions are drawn the significance of the factors.

Keywords: elastic multi-layered half space; Green's function; wavenumber domain; spatial domain; Precise Integration Method (PIM); impedance functions

1. Introduction

An important step in the study of dynamic interaction between the structure and the supporting medium is the evaluation of the dynamic response for a massless foundation supported on the soil. It plays an important role in the study of machine vibration as well as in the study of structural response to earthquake excitations. The problem is a mixed-boundary-value issue in which the displacements are prescribed under the foundation while the rest of the surface is traction free. Over the past decades, a considerable amount of works have been done on this problem. Different approaches were developed.

Among all the approaches, the analytical solutions always have theoretical appeal in themselves, they are really important as tools in the solution of the involved boundary value problems arising in seismology and Geo-mechanics. Luco and Westmann (1971), Veletsos *et al.* (1971, 1973) presented analytical solutions for the vibration of a circular foundation on an elastic

*Corresponding author, Ph.D. Student, E-mail: lin.chen@lbb.rwth-aachen.de

homogeneous half space. They reduced the resulting mixed-boundary-value problem by standard technique to the solution of Fredholm integral equation. Later, Luco (1975) extended his solutions to an elastic multi-layered half space. Further, Gazetas (1980, 1981) applied the Fredholm integral equation to analyze the dynamic response of a strip foundation on a multi-layered half space. Luco and Mita (1987) used the integral representation involving the free-field ground motion to calculate the dynamic force-displacement relation of the foundation. However, the analytical solutions available so far are restricted to the analysis of the foundation with relatively simple geometry.

For an irregularly shaped foundation, one should employ numerical methods to analyze the dynamic response of the foundation. Finite element method (FEM) is one of the most widely used approaches. The application of FEM in this problem needs to represent the semi-infinite soil medium by a finite size model. This model will have the effect of trapping the energy of the system in a finite region. Furthermore, it will impart to the continuum some artificial dynamic characteristics (Lehmann 2005). These effects may be overcome by the use of infinite elements (Kazakov 2010) or by the use of energy transmitting boundaries (Lee *et al.* 2011). Several types of finite elements are available for the dynamic response analysis of the foundation: three-dimensional solid elements (Ju *et al.* 2012); axisymmetric solid elements (Said *et al.* 2009); and two-dimensional plane strain elements (Ellis *et al.* 2001, Kim *et al.* 2003). In principle, FEM can be used to solve a large class of problems. In particular, its use should be invoked for problems involving non-regular foundation shapes, inclined layering in soil deposits, complex constitutive relation, embedment effects, coupling between adjacent foundations. However, the problems encountered in the design of large-scale structures restrict the use of FEM. This is due to the fact that the transmitting boundary should be placed far away from the soil-structure interface. Furthermore, to be able to transmit higher frequencies, sufficiently small-sized elements must be used. The combined effect of these two requirements leads to prohibitive costs and severely taxes the storage memory capabilities of presently available computer hardware.

The boundary element method (BEM) is well suited to model infinite medium because it is able to take into account the wave radiation to infinity. It has been used to calculate the dynamic impedance functions of rectangular (Dominguez *et al.* 1978), circular (Alarcón *et al.* 1989) and strip foundation in the frequency domain (Abascal *et al.* 1986) as well as in the time domain (Spyrakos *et al.* 1986, Karabalis *et al.* 2006). Recently, a new boundary element formulation is proposed for the wave load analysis of submerged or floating foundation (Yalcin *et al.* 2013). However, for the boundary element method, the required fundamental solution is not always available.

In view of the limitations by applying the finite element method (FEM) and boundary element method (BEM), the combination of BEM with FEM was emerged to eliminate their shortcomings. Normally, the structure and a small portion of the supporting soil can be discretized by finite elements, while the remaining soil medium is represented by boundary elements. Karabalis and Beskos (1985) analyzed the response of three-dimensional linear elastic foundation of arbitrary shape with this approach. Estorff and Firuziaan (2000) proposed a general coupled boundary element/finite element formulation for the investigation of dynamic soil-structure interaction including nonlinearities. Rizos and Wang (2002) used the coupled methodology for the 3D wave propagation and soil-structure interaction analysis in the direct time domain. Sheng *et al.* (2006) employed the wavenumber finite/boundary element method, which is formulated in terms of the wavenumber, to predict the ground motion from the trains. Recently, Galvín *et al.* (2010) presented a generally three dimensional multi-body-finite element-boundary element model, formulated in

the time domain to predict vibrations due to train passage at the vehicle, the track and the free field. Later, Romero *et al.* (2013) considered the non-linear contact at the FEM/BEM interface to analyze the dynamic response of rectangular foundation. However, in general, the equation of the coupled system has a banded structure only in the FEM part, while in the BEM part it is fully populated. Consequently, for its solution the optimized solvers usually used in FEM cannot be employed anymore, which leads to rather expensive calculations regarding the computation time.

The purpose of this study is to present an efficient method that will permit analyzing the forced vibration of a rigid surface foundation with arbitrary shape, in which it concentrates mainly on the derivation of the dynamic impedance and compliance functions of the foundation. The development of the method has been guided by the desire to accomplish the following objectives, and it should be:

- (1) valid for the wide range of frequency interested in the seismology and engineering.
- (2) suitable for the dynamic analysis of foundation with arbitrary shape.
- (3) stable for models involving solid layers of thicknesses ranging from large value to thin ones.

To meet these objectives, it divides the contact area between the foundation and ground into a number of sub square-elements. The contact forces within each area are assumed as concentrated loads, which are applied at the center of the sub square-elements. And the force-displacement relation within each sub-element is expressed as the Green's function, which is obtained by the Fourier-Bessel transform and Precise Integration Method (PIM) (Zhong 2004). PIM is an efficient and accurate numerical method for the solution of one order ordinary differential equation, which is widely employed in the field of structural dynamics (Zhong *et al.* 2001, Zhang *et al.* 2012) and wave propagation analysis (Gao *et al.* 2006, Lin *et al.* 2013a, Lin *et al.* 2013b, Lin *et al.* 2014). Considering the displacement boundary conditions, it obtains a system of linear algebraic equation in terms of the contact forces at each sub-element. Also, employing the force equilibrium of the foundation, one can obtain the relation between the total forces of the foundation and the contact forces at each sub-element. Combining the displacement boundary conditions and force equilibrium, it leads to the desired dynamic impedance functions of the foundation. Numerical examples are provided in the last part of the paper. The accuracy of the method is validated by comparison to the solutions available in the literature. Also, parametric studies on the dynamic response of foundation are investigated.

An outline of this paper follows: In Section 2, the solution procedure for wave motion equation of layered half space is addressed. Both the Green's function in the wavenumber domain and spatial domain are derived. In Section 3, the impedance functions of arbitrarily shaped foundation are calculated. In Section 4, three numerical examples are presented. The first two cases are used to validate the proposed approach. The last one is employed to demonstrate the capability of the approach. Parametric studies are performed in Section 5. Here, it investigates the effects of Poisson's ratio, material damping and contact condition of soil-foundation interface on the impedance and compliance functions. The paper ends with some concluding remarks.

2. Dynamic response of multi-layered half-space

2.1 Basic equation of wave propagation

Consider an arbitrarily shaped rigid foundation placed on a homogeneous, isotropic half space overlaid by n parallel layers of similar medium but with distinct material properties, see Fig. 1. A

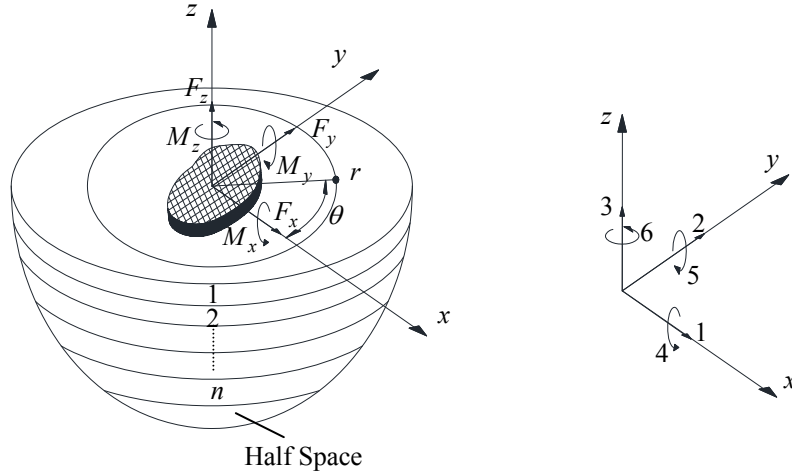


Fig. 1 Rigid foundation on a multi-layered half space

cylindrical coordinate system is set at the top free surface and the origin is placed at the center of the foundation. The j th layer is characterized by the material parameters: λ_j and μ_j (Lame constants), ρ_j (mass density), ζ_j (material damping ratio) and thickness $h_j=z_j-z_{j-1}$, where z_j and z_{j-1} are the depths of its upper and lower interfaces. The Lamé constants, mass density and material damping ratio of the half space are denoted as λ_H, μ_H, ρ_H and ζ_H .

In the cylindrical coordinate system, the general differential equation of wave motion is

$$\begin{aligned} \sigma_{r,r} + \frac{1}{r} \tau_{\theta r, \theta} + \tau_{zr,z} + \frac{\sigma_r - \sigma_\theta}{r} &= \rho \frac{\partial^2 u_r}{\partial t^2} \\ \tau_{r\theta,r} + \frac{1}{r} \sigma_{\theta,\theta} + \tau_{z\theta,z} + \frac{2\tau_{r\theta}}{r} &= \rho \frac{\partial^2 u_\theta}{\partial t^2} & \tau_{rz,r} + \frac{1}{r} \tau_{\theta z, \theta} + \sigma_{z,z} + \frac{\tau_{rz}}{r} &= \rho \frac{\partial^2 u_z}{\partial t^2} \end{aligned} \tag{1}$$

Herein the normal and shear stress are denoted as σ and τ . As usual, the first subscript of τ denotes the direction of the stress component; the second one is the direction of the normal of the infinitesimal area that the stress component acts on. u_r, u_θ and u_z are radial, tangential and vertical displacement. The comma denotes a partial derivative. The problem is solved in the frequency domain. The variation with time is given by the factor $\exp(i\omega t)$.

Since the material is isotropic, the wave motion equation can be decoupled into in-plane wave motion (P-SV wave) and out-of-plane wave motion (SH wave) in the transformed wavenumber domain (Kausel 2006). The transformations are based on the Fourier-Bessel transform.

$$\mathbf{S}(r, \theta, z) = \sum_{n=0}^{\infty} \mathbf{T}(n\theta) \int_{k=0}^{\infty} k \mathbf{C}_n(kr) \bar{\mathbf{S}}(k, n) dk \quad \bar{\mathbf{S}}(k, n) = a_n \int_{r=0}^{\infty} r \mathbf{C}_n(kr) \int_{\theta=0}^{2\pi} \mathbf{T}(n\theta) \mathbf{S}(r, \theta, z) dr d\theta \tag{2}$$

where $\bar{\mathbf{S}}(k, n) = \{\bar{\tau}_{rz} \quad \bar{\tau}_{\theta z} \quad \bar{\sigma}_z\}^T$ denotes the stress vector in the transformed wavenumber domain, The superscript bar is a reminder that the components are defined in the wavenumber domain; $\mathbf{S}(r, \theta, z) = \{\tau_{rz} \quad \tau_{\theta z} \quad \sigma_z\}^T$ refers to the value in the spatial domain. Similar domain transformation can be performed for the displacement vector $\mathbf{U} = \{u_r \quad u_\theta \quad u_z\}^T$ as Eq. (2). The orthogonalization factor a_n is the normalization factor, which is equal to $1/2\pi$ for $n=0$ and $1/\pi$ for $n \neq 0$. The diagonal matrix

$\mathbf{T}(n\theta)$ is $\mathbf{T}(n\theta)=\text{diag}[\cos n\theta \quad -\sin n\theta \quad \cos n\theta]$ for the symmetric case about the x axis (r -axis at $\theta=0$); and is $\mathbf{T}(n\theta)=\text{diag}[\sin n\theta \quad \cos n\theta \quad \sin n\theta]$ for the anti-symmetric case. θ is the angle of revolution around x axis. The matrix $\mathbf{C}_n(kr)$ includes Bessel functions, which is

$$\mathbf{C}_n(kr) = \frac{1}{kr} \begin{bmatrix} r \frac{d}{d(kr)} J_n(kr) & nJ_n(kr) & 0 \\ nJ_n(kr) & r \frac{d}{d(kr)} J_n(kr) & 0 \\ 0 & 0 & -krJ_n(kr) \end{bmatrix} \quad (3)$$

in which $J_n(kr)$ is the first kind Bessel function with n th order.

For the evaluation of Green's function, only the cases of $n=0$ and $n=1$ of Eq. (2) need to be considered (Kausel 1981). The case $n=0$ corresponds to an axisymmetric vertical load case, while the case $n=1$ is used to the horizontal load case which is symmetric about the x axis.

After Fourier-Bessel transform of Eq. (1), the in-plane wave motion and out-of-plane wave motion equation will be obtained. In-plane wave motion corresponds to the displacement $\bar{u}_r(k,z)$ and $\bar{u}_z(k,z)$. The corresponding equations are (Kausel 2006).

$$\mu \bar{u}_r''(k) - ik(\lambda + \mu) \bar{u}_z'(k) - [(\lambda + 2\mu)k^2 - \rho\omega^2] \bar{u}_r(k) = 0 \quad (\lambda + 2\mu) \bar{u}_z''(k) - ik(\lambda + \mu) \bar{u}_r'(k) - (\mu k^2 - \rho\omega^2) \bar{u}_z(k) = 0 \quad (4)$$

Out-of-plane wave motion corresponds to the displacement $\bar{u}_\theta(k)$

$$\mu \bar{u}_\theta''(k) - (k^2 \mu - \rho\omega^2) \bar{u}_\theta(k) = 0 \quad (5)$$

In Eqs. (4) and (5), $(\cdot)' = \partial(\cdot)/\partial z$; hereinafter, the superscript prime of $(\cdot)'$ has the identical definition. Eqs. (4) and (5) can be written in a matrix form as

$$\mathbf{K}_{22} \bar{\mathbf{U}}'' + (\mathbf{K}_{21} - \mathbf{K}_{12}) \bar{\mathbf{U}}' - (\mathbf{K}_{11} - \rho\omega^2 \mathbf{I}) \bar{\mathbf{U}} = \mathbf{0} \quad (6)$$

where $\bar{\mathbf{U}} = \{\bar{u}_r \quad \bar{u}_\theta \quad \bar{u}_z\}^T$ is the displacement vector in the wavenumber domain; \mathbf{I} is a 3×3 unit matrix. The coefficient matrices are

$$\mathbf{K}_{11} = k^2 \begin{bmatrix} \lambda + 2\mu & 0 & 0 \\ 0 & \mu & 0 \\ 0 & 0 & \mu \end{bmatrix} \quad \mathbf{K}_{21} = \mathbf{K}_{12}^H = ik \begin{bmatrix} 0 & 0 & \mu \\ 0 & 0 & 0 \\ \lambda & 0 & 0 \end{bmatrix} \quad \mathbf{K}_{22} = \begin{bmatrix} \mu & 0 & 0 \\ 0 & \mu & 0 \\ 0 & 0 & \lambda + 2\mu \end{bmatrix} \quad (7)$$

in which the superscript H denotes the Hermitian transpose. For a viscoelastic medium with a hysteretic type dissipative mechanism, one only needs to replace λ and μ by the complex Lamé parameters $\lambda(1+2\zeta i)$ and $\mu(1+2\zeta i)$, where ζ is the hysteretic damping ratio.

Writing Eq. (6) in a variation form, $\Gamma(\bar{\mathbf{U}}, \bar{\mathbf{U}}')$ is the Lagrange function.

$$\Gamma(\bar{\mathbf{U}}, \bar{\mathbf{U}}') = \bar{\mathbf{u}}'^T \mathbf{K}_{22} \bar{\mathbf{U}}' / 2 + \bar{\mathbf{U}}'^T \mathbf{K}_{21} \bar{\mathbf{U}} + \bar{\mathbf{U}}^T (\mathbf{K}_{11} - \rho\omega^2 \mathbf{I}) \bar{\mathbf{U}} \quad \delta \int_V \Gamma(\bar{\mathbf{U}}, \bar{\mathbf{U}}') dz = 0 \quad (8)$$

In order to solve Eq. (6), it is necessary to reduce the second order differential equation to first order. Here, the dual vector is introduced, which is the stress vector $\bar{\mathbf{S}}$.

$$\bar{\mathbf{S}} = \partial\Gamma/\partial\bar{\mathbf{U}}' = (\mathbf{K}_{22}\bar{\mathbf{U}}' + \mathbf{K}_{21}\bar{\mathbf{U}}) \tag{9}$$

Substituting Eq. (9) into (6), it can be written as the following partitioned form

$$\Psi' = \begin{Bmatrix} \bar{\mathbf{U}} \\ \bar{\mathbf{S}} \end{Bmatrix}' = \mathbf{\Pi}\Psi = \begin{bmatrix} \mathbf{A} & \mathbf{D} \\ \mathbf{B} & \mathbf{C} \end{bmatrix} \begin{Bmatrix} \bar{\mathbf{U}} \\ \bar{\mathbf{S}} \end{Bmatrix} \tag{10}$$

in which

$$\mathbf{A} = -\mathbf{K}_{22}^{-1}\mathbf{K}_{21} = -\mathbf{C}^H \quad \mathbf{B} = \mathbf{K}_{11} - \mathbf{K}_{12}\mathbf{K}_{22}^{-1}\mathbf{K}_{21} - \rho\omega^2\mathbf{I} \quad \mathbf{D} = \mathbf{K}_{22}^{-1} \tag{11}$$

The matrix $\mathbf{\Pi}$ in Eq. (10) is

$$\mathbf{H} = \begin{bmatrix} 0 & 0 & -ik & 1/\mu & 0 & 0 & 0 \\ 0 & 0 & 0 & 0 & 0 & 1/\mu & 0 \\ -ik\lambda/(\lambda+2\mu) & 0 & 0 & 0 & 0 & 0 & 1/\lambda+2\mu \\ 4k^2\mu(\lambda+\mu)/(\lambda+2\mu) - \rho\omega^2 & 0 & 0 & 0 & 0 & 0 & -ik\lambda/(\lambda+2\mu) \\ 0 & k^2\mu - \rho\omega^2 & 0 & 0 & 0 & 0 & 0 \\ 0 & 0 & -\rho\omega^2 & -ik & 0 & 0 & 0 \end{bmatrix} \tag{12}$$

For perfectly incompressible material (Poisson's ratio $\nu=0.5$), λ is infinite. Eq. (12) is modified as

$$\mathbf{\Pi} = \begin{bmatrix} 0 & 0 & -ik & 1/\mu & 0 & 0 & 0 \\ 0 & 0 & 0 & 0 & 1/\mu & 0 & 0 \\ -ik & 0 & 0 & 0 & 0 & 0 & 0 \\ 4k^2\mu - \rho\omega^2 & 0 & 0 & 0 & 0 & 0 & -ik \\ 0 & k^2\mu - \rho\omega^2 & 0 & 0 & 0 & 0 & 0 \\ 0 & 0 & -\rho\omega^2 & -ik & 0 & 0 & 0 \end{bmatrix} \tag{13}$$

The continuity conditions at interfaces between two layers are $\bar{\mathbf{U}}_i^+ = \bar{\mathbf{U}}_i^-$, $\bar{\mathbf{S}}_i^+ = \bar{\mathbf{S}}_i^-$ ($i=1,2,\dots,n-1,n$).

2.2 Wave motion in the half space

Two cases of layered half space are considered: the layered medium on a rigid base and on a semi-infinite space. When the layered medium underlain by a rigid base, there is no displacement at the bottom surface. The boundary condition is $\bar{\mathbf{U}}=\mathbf{0}$ ($z=z_n$). In another case, the radiation conditions should be considered. The state equation for the semi-infinite space, i.e., the $(n+1)$ th layer, is $\Psi'_{n+1} = \mathbf{\Pi}_{n+1}\Psi_{n+1}$. If $\bar{\mathbf{T}}_{n+1}$ and $\bar{\mathbf{\Lambda}}_{n+1}$ is the eigenvector and eigenvalue matrix of the matrix Ψ_{n+1} , then

$$\Psi'_{n+1} = \bar{\mathbf{T}}_{n+1}\bar{\mathbf{\Lambda}}_{n+1}\bar{\mathbf{T}}_{n+1}^{-1}\Psi_{n+1} \tag{14}$$

$$\bar{\mathbf{\Lambda}}_{n+1} = \text{diag}[\alpha_2, \alpha_1, \alpha_1, -\alpha_2, -\alpha_1, -\alpha_1] \tag{15}$$

$$\alpha_1 = \sqrt{k^2 - \rho_H\omega^2/\mu_H} \quad \alpha_2 = \sqrt{k^2 - \rho_H\omega^2/(\lambda_H + 2\mu_H)} \tag{16}$$

$$\bar{\mathbf{T}}_{n+1} = \begin{bmatrix} \bar{\mathbf{T}}_{uu} & \bar{\mathbf{T}}_{ud} \\ \bar{\mathbf{T}}_{du} & \bar{\mathbf{T}}_{dd} \end{bmatrix} = \begin{bmatrix} -ik & 0 & -\alpha_1 & ik & 0 & -\alpha_1 \\ 0 & 1 & 0 & 0 & 1 & 0 \\ \alpha_2 & 0 & -ik & \alpha_2 & 0 & ik \\ i2\mu_H k \alpha_2 & 0 & 2k^2 \mu_H - \rho_H \omega^2 & i2\mu_H k \alpha_2 & 0 & \rho_H \omega^2 - 2k^2 \mu_H \\ 0 & -\alpha_1 \mu_H & 0 & 0 & \alpha_1 \mu_H & 0 \\ \rho_H \omega^2 - 2k^2 \mu_H & 0 & i2\mu_H k \alpha_1 & 2k^2 \mu_H - \rho_H \omega^2 & 0 & i2\mu_H k \alpha_1 \end{bmatrix} \quad (17)$$

For the perfectly incompressible material (Poisson’s ratio $\nu=0.5$), Eq. (16) should be modified as

$$\alpha_1 = \sqrt{k^2 - (\rho_H \omega^2 / \mu_H)} \quad \alpha_2 = k \quad (18)$$

The radiation conditions require no upward wave in the semi-infinite space, which yields

$$\bar{\mathbf{S}}(z_n) = \bar{\mathbf{T}}_{dd} \bar{\mathbf{T}}_{ud}^{-1} \bar{\mathbf{U}}(z_n) = \bar{\mathbf{R}}_\infty \bar{\mathbf{U}}(z_n) \quad (19)$$

Eq. (19) is the general stress-displacement relation for the semi-infinite space. If we consider different values of wavenumber k and frequency ω , the following specific equation can be obtained

(a) Non-zero frequency, non-zero wavenumber: $k>0, \omega>0$

$$\bar{\mathbf{R}}_\infty = \frac{\rho_H \omega^2}{k^2 - \alpha_1 \alpha_2} \begin{bmatrix} \alpha_2 & 0 & -ik \\ 0 & 0 & 0 \\ ik & 0 & \alpha_1 \end{bmatrix} + \begin{bmatrix} 0 & 0 & 2ik \mu_H \\ 0 & \mu_H \alpha_1 & 0 \\ -2ik \mu_H & 0 & 0 \end{bmatrix} \quad (20)$$

(b) Zero frequency, non-zero wavenumber: $k>0, \omega=0$

For this case, one cannot directly set the frequency $\omega>0$ in Eq. (17), because there is no inverse matrix of $\bar{\mathbf{T}}_{ud}$. To overcome this, the limit approaching method is employed to Eq. (20). Utilizing l’Hospital’s rule, the following expression can be obtained

$$\bar{\mathbf{R}}_\infty = \frac{k \mu_H}{\lambda_H + 3\mu_H} \begin{bmatrix} 2(\lambda_H + 2\mu_H) & 0 & i2\mu_H \\ 0 & \lambda_H + 3\mu_H & 0 \\ -i2\mu_H & 0 & 2(\lambda_H + 2\mu_H) \end{bmatrix} \quad (21)$$

(a) Non-zero frequency, zero wavenumber: $k=0, \omega>0$

$$\bar{\mathbf{R}}_\infty = \text{diag} \left[i\omega \sqrt{\rho_H \mu_H} \quad i\omega \sqrt{\rho_H \mu_H} \quad i\omega \sqrt{\rho_H (\lambda_H + 2\mu_H)} \right] \quad (22)$$

(b) Zero frequency, zero wavenumber: $k=0, \omega=0$. $\bar{\mathbf{R}}_\infty = \text{diag}[0 \quad 0 \quad 0]$

2.3 Solution procedure for layered medium

Within an arbitrary layer, select an interval $[z_a, z_b]$ ($z_a < z_b$), and assume that it is subjected to external dynamic tractions, $\bar{\mathbf{p}}_a$ and $\bar{\mathbf{p}}_b$, at its upper and lower external interfaces. Hence, if $\bar{\mathbf{U}}_a$ and $\bar{\mathbf{U}}_b$ are the displacements at the two interfaces of the layer, we have (Kausel 2006)

$$\begin{Bmatrix} \bar{\mathbf{p}}_a \\ \bar{\mathbf{p}}_b \end{Bmatrix} = \mathbf{K} \begin{Bmatrix} \bar{\mathbf{U}}_a \\ \bar{\mathbf{U}}_b \end{Bmatrix} = \begin{bmatrix} \mathbf{K}_{aa} & \mathbf{K}_{ab} \\ \mathbf{K}_{ba} & \mathbf{K}_{bb} \end{bmatrix} \begin{Bmatrix} \bar{\mathbf{U}}_a \\ \bar{\mathbf{U}}_b \end{Bmatrix} \quad (23)$$

in which, \mathbf{K} is the stiffness of the layer.

The dynamic potential energy of the layer is

$$\Omega = \frac{1}{2} \{ \bar{\mathbf{U}}_a \quad \bar{\mathbf{U}}_b \} \mathbf{K} \{ \bar{\mathbf{U}}_a \quad \bar{\mathbf{U}}_b \}^T \quad (24)$$

The corresponding internal force vectors $\bar{\mathbf{S}}_a$ and $\bar{\mathbf{S}}_b$ can be introduced from the principle of virtual work, $\bar{\mathbf{S}} = \partial\Omega/\partial\bar{\mathbf{U}}$. Hence, $\bar{\mathbf{S}}_a$ and $\bar{\mathbf{S}}_b$ can be derived from Eq. (24) as

$$\bar{\mathbf{S}}_a = \partial\Omega/\partial\bar{\mathbf{U}}_a = \mathbf{K}_{aa}\bar{\mathbf{U}}_a + \mathbf{K}_{ab}\bar{\mathbf{U}}_b \quad \bar{\mathbf{S}}_b = -\partial\Omega/\partial\bar{\mathbf{U}}_b = -\mathbf{K}_{ba}\bar{\mathbf{U}}_a - \mathbf{K}_{bb}\bar{\mathbf{U}}_b \quad (25)$$

Solving Eq. (25), we will obtain

$$\bar{\mathbf{U}}_b = \mathbf{F}\bar{\mathbf{U}}_a - \mathbf{G}\bar{\mathbf{S}}_b \quad \bar{\mathbf{S}}_a = \mathbf{Q}\bar{\mathbf{U}}_a + \mathbf{E}\bar{\mathbf{S}}_b \quad (26)$$

which implies that the stress-displacement relation at the two ends of one layer is linearly correlated. Also, \mathbf{F} , \mathbf{G} , \mathbf{Q} and \mathbf{E} are termed as correlation matrices of the layer, which can be obtained from Eq. (25). However, the matrix \mathbf{K} is unknown. Thus, they cannot be obtained explicitly here. It will solve the correlation matrices \mathbf{F} , \mathbf{G} , \mathbf{Q} and \mathbf{E} by Precise Integration Method (PIM) (Zhong 2004) latter.

Considering any two adjacent layers 1 and 2 ranging $[z_a, z_b]$ and $[z_b, z_c]$, now, we apply Eq. (26) to the two layers to merge into a new layer c ranging $[z_a, z_c]$ with the continuity condition at interface between them. The corresponding correlation matrices for the newly combined layer c are

$$\mathbf{F}_c = \mathbf{F}_2(\mathbf{I} + \mathbf{G}_1\mathbf{Q}_2)^{-1}\mathbf{F}_1, \quad \mathbf{G}_c = \mathbf{G}_2 + \mathbf{F}_2(\mathbf{G}_1^{-1} + \mathbf{Q}_2)^{-1}\mathbf{E}_2, \quad \mathbf{Q}_c = \mathbf{Q}_1 + \mathbf{E}_1(\mathbf{Q}_2^{-1} + \mathbf{G}_1)^{-1}\mathbf{F}_1, \quad \mathbf{E}_c = \mathbf{E}_1(\mathbf{I} + \mathbf{Q}_2\mathbf{G}_1)^{-1}\mathbf{E}_2 \quad (27)$$

where the subscripts 1, 2 and c denote the corresponding layer that the correlation matrices belong to.

Since $\bar{\mathbf{U}}_a$ and $\bar{\mathbf{S}}_b$ are mutually independent in Eq. (26), differentiating it with respect to z_b and comparing with Eq. (10), one can obtain a set of ordinary differential equations

$$\mathbf{F}' = (\mathbf{A} + \mathbf{GB})\mathbf{F} \quad \mathbf{G}' = \mathbf{AG} - \mathbf{GC} - \mathbf{D} + \mathbf{GBG} \quad \mathbf{Q}' = -\mathbf{EBF} \quad \mathbf{E}' = \mathbf{E}(\mathbf{BG} - \mathbf{C}) \quad (28)$$

Let z_b approach z_a , the boundary conditions for these equations are

$$\mathbf{E}(z_a, z_a) = \mathbf{F}(z_a, z_a) = \mathbf{I} \quad \mathbf{G}(z_a, z_a) = \mathbf{Q}(z_a, z_a) = \mathbf{0} \quad (29)$$

Eq. (28) shows the matrices \mathbf{F} , \mathbf{G} , \mathbf{Q} and \mathbf{E} are coupled with each other. In order to obtain them, the Precise Integration Method (PIM) (Zhong 2004, Gao 2006) will be employed. The detailed theoretical derivation of the method can be found in the work of Zhong. Here, only the application of the method in the present study will be addressed. For an arbitrary i th layer ($i=1,2,\dots,n$) of the layered medium, it assumes the thickness of the layer being h_i . The layer is firstly divided into 2^{N_1} (N_1 is an integer) sub-layers of equal thickness $\bar{h}_i = h_i/2^{N_1}$, and each sub-layer is further divided into 2^{N_2} (N_2 is an integer) mini-layers of equal thickness $\tau = \bar{h}_i/2^{N_2}$. In this paper, $N_1=20$ and $N_2=20$ are chosen. Under such condition, the thickness of the mini-layers is

$\tau = \bar{h}_i / 2^{N_2} = h_i / 2^{N_1+N_2} = h_i / (1048576 \times 1048576)$. Since the thickness τ of such intervals is sufficiently small, the correlation matrices $\mathbf{F}(\tau)$, $\mathbf{G}(\tau)$, $\mathbf{Q}(\tau)$ and $\mathbf{E}(\tau)$ can be expressed in terms of the Taylor series expansion to ensure sufficient accuracy. Any desired accuracy of the results can be achieved with increasing terms of the expansion. In this paper, four terms of Taylor series are considered. The Taylor series expansion is truncated after the τ^4 terms. Therefore, the relative order of the neglected terms is τ^4 . With $N_2=20$, τ has been divided by even more than 10^6 . Thus τ^4 will be of the order 10^{-24} , which is well beyond the precision of real*8 typically only the leftmost 15 digits significant.

$$\begin{aligned} \tilde{\mathbf{F}}(\tau) &\approx \mathbf{f}_1\tau + \mathbf{f}_2\tau^2 + \mathbf{f}_3\tau^3 + \mathbf{f}_4\tau^4 & \mathbf{F}(\tau) &= \mathbf{I} + \tilde{\mathbf{F}}(\tau) & \mathbf{Q}(\tau) &\approx \boldsymbol{\theta}_1\tau + \boldsymbol{\theta}_2\tau^2 + \boldsymbol{\theta}_3\tau^3 + \boldsymbol{\theta}_4\tau^4 \\ \tilde{\mathbf{E}}(\tau) &\approx \boldsymbol{\varphi}_1\tau + \boldsymbol{\varphi}_2\tau^2 + \boldsymbol{\varphi}_3\tau^3 + \boldsymbol{\varphi}_4\tau^4 & \mathbf{E}(\tau) &= \mathbf{I} + \tilde{\mathbf{E}}(\tau) & \mathbf{G}(\tau) &\approx \boldsymbol{\gamma}_1\tau + \boldsymbol{\gamma}_2\tau^2 + \boldsymbol{\gamma}_3\tau^3 + \boldsymbol{\gamma}_4\tau^4 \end{aligned} \quad (30)$$

where $\boldsymbol{\theta}_i$, $\boldsymbol{\gamma}_i$, \mathbf{f}_i and $\boldsymbol{\varphi}_i$ ($i=1,2,3,4$) are the coefficient matrices to be determined. Substituting Eq. (30) into (28), the coefficients of various τ must be equal to zero, which leads to

$$\boldsymbol{\theta}_1 = -\mathbf{B} \quad \boldsymbol{\gamma}_1 = -\mathbf{D} \quad \mathbf{f}_1 = \mathbf{A} \quad \boldsymbol{\varphi}_1 = -\mathbf{C} \quad (31)$$

$$\boldsymbol{\theta}_2 = -(\boldsymbol{\varphi}_1\mathbf{B} + \mathbf{B}\mathbf{f}_1)/2 \quad \boldsymbol{\gamma}_2 = (\mathbf{A}\boldsymbol{\gamma}_1 - \boldsymbol{\gamma}_1\mathbf{C})/2 \quad \mathbf{f}_2 = (\mathbf{A}\mathbf{f}_1 + \boldsymbol{\gamma}_1\mathbf{B})/2 \quad \boldsymbol{\varphi}_2 = (\mathbf{B}\boldsymbol{\gamma}_1 - \boldsymbol{\varphi}_1\mathbf{C})/2 \quad (32)$$

$$\boldsymbol{\theta}_3 = -(\boldsymbol{\varphi}_2\mathbf{B} + \mathbf{B}\mathbf{f}_2 + \boldsymbol{\varphi}_1\mathbf{B}\mathbf{f}_1)/3 \quad \boldsymbol{\gamma}_3 = (\mathbf{A}\boldsymbol{\gamma}_2 - \boldsymbol{\gamma}_2\mathbf{C} + \boldsymbol{\gamma}_1\mathbf{B}\boldsymbol{\gamma}_1)/3 \quad \mathbf{f}_3 = (\mathbf{A}\mathbf{f}_2 + \boldsymbol{\gamma}_2\mathbf{B} + \boldsymbol{\gamma}_1\mathbf{B}\mathbf{f}_1)/3 \quad \boldsymbol{\varphi}_3 = (\mathbf{B}\boldsymbol{\gamma}_2 - \boldsymbol{\varphi}_2\mathbf{C} + \boldsymbol{\varphi}_1\mathbf{B}\boldsymbol{\gamma}_1)/3 \quad (33)$$

$$\begin{aligned} \boldsymbol{\theta}_4 &= -(\boldsymbol{\varphi}_3\mathbf{B} + \mathbf{B}\mathbf{f}_3 + \boldsymbol{\varphi}_2\mathbf{B}\mathbf{f}_1 + \boldsymbol{\varphi}_1\mathbf{B}\mathbf{f}_2)/4 & \boldsymbol{\gamma}_4 &= (\mathbf{A}\boldsymbol{\gamma}_3 - \boldsymbol{\gamma}_3\mathbf{C} + \boldsymbol{\gamma}_2\mathbf{B}\boldsymbol{\gamma}_1 + \boldsymbol{\gamma}_1\mathbf{B}\boldsymbol{\gamma}_2)/4 \\ \mathbf{f}_4 &= (\mathbf{A}\mathbf{f}_3 + \boldsymbol{\gamma}_3\mathbf{B} + \boldsymbol{\gamma}_2\mathbf{B}\mathbf{f}_1 + \boldsymbol{\gamma}_1\mathbf{B}\mathbf{f}_2)/4 & \boldsymbol{\varphi}_4 &= (\mathbf{B}\boldsymbol{\gamma}_3 - \boldsymbol{\varphi}_3\mathbf{C} + \boldsymbol{\varphi}_1\mathbf{B}\boldsymbol{\gamma}_2 + \boldsymbol{\varphi}_2\mathbf{B}\boldsymbol{\gamma}_1)/4 \end{aligned} \quad (34)$$

The matrixes $\tilde{\mathbf{F}}(\tau)$ and $\tilde{\mathbf{E}}(\tau)$ are extremely small compared to the unit matrix \mathbf{I} in the small interval τ . Therefore, it is important that they are computed and stored independently to avoid losing effective digits. The derivations in the former sections are exact, the only approximation made in the Precise Integration Method (PIM) is the truncation of the Taylor series expansion in Eq. (30). It will cause numerical errors; however, the errors are less than the round-off error of double precision computation. Therefore, the method is exact in the sense that any method can be exact, i.e., it is as exact as the computer precision permits. Once $\mathbf{F}(\tau)$, $\mathbf{G}(\tau)$, $\mathbf{Q}(\tau)$ and $\mathbf{E}(\tau)$ for a mini-layer are determined, they are combined as below. Considering that, all mini-layers within one sub-layer have equal thickness and identical material properties, therefore, $\mathbf{F}_1=\mathbf{F}_2=\mathbf{F}$, $\mathbf{G}_1=\mathbf{G}_2=\mathbf{G}$, $\mathbf{Q}_1=\mathbf{Q}_2=\mathbf{Q}$ and $\mathbf{E}_1=\mathbf{E}_2=\mathbf{E}$. Considering $\tilde{\mathbf{F}}_c$ and $\tilde{\mathbf{E}}_c$ being very small, for combination of mini-layers, Eq. (27) is modified as

$$\begin{aligned} \mathbf{Q}_c &= \mathbf{Q} + (\mathbf{I} + \tilde{\mathbf{E}})(\mathbf{Q}^{-1} + \mathbf{G})^{-1}(\mathbf{I} + \tilde{\mathbf{F}}) & \mathbf{G}_c &= \mathbf{G} + (\mathbf{I} + \tilde{\mathbf{F}})^{-1}(\mathbf{G}^{-1} + \mathbf{Q})^{-1}(\mathbf{I} + \tilde{\mathbf{E}}) \\ \tilde{\mathbf{F}}_c &= (\tilde{\mathbf{F}} - \mathbf{G}\mathbf{Q}/2)(\mathbf{I} + \mathbf{G}\mathbf{Q})^{-1} + (\mathbf{I} + \mathbf{G}\mathbf{Q})^{-1}(\tilde{\mathbf{F}} - \mathbf{G}\mathbf{Q}/2) + \tilde{\mathbf{F}}(\mathbf{I} + \mathbf{G}\mathbf{Q})^{-1}\tilde{\mathbf{F}} & \mathbf{F}_c &= \mathbf{I} + \tilde{\mathbf{F}}_c \\ \tilde{\mathbf{E}}_c &= (\tilde{\mathbf{E}} - \mathbf{Q}\mathbf{G}/2)(\mathbf{I} + \mathbf{Q}\mathbf{G})^{-1} + (\mathbf{I} + \mathbf{Q}\mathbf{G})^{-1}(\tilde{\mathbf{E}} - \mathbf{Q}\mathbf{G}/2) + \tilde{\mathbf{E}}(\mathbf{I} + \mathbf{Q}\mathbf{G})^{-1}\tilde{\mathbf{E}} & \mathbf{E}_c &= \mathbf{I} + \tilde{\mathbf{E}}_c \end{aligned} \quad (35)$$

Recursively executing Eq. (35) N_2 times, the matrices \mathbf{F} , \mathbf{G} , \mathbf{Q} and \mathbf{E} turn to be the correlation matrices $\mathbf{F}(\bar{h}_i)$, $\mathbf{G}(\bar{h}_i)$, $\mathbf{Q}(\bar{h}_i)$ and $\mathbf{E}(\bar{h}_i)$ of the given \bar{h}_i interval. Such algorithm is termed as ‘interval doubling’. Since the matrices $\tilde{\mathbf{F}}$ and $\tilde{\mathbf{E}}$ of \bar{h}_i interval are no longer very small, repeatedly employing Eq. (27) N_1 times, the correlation matrices $\mathbf{F}(h_i)$, $\mathbf{G}(h_i)$, $\mathbf{Q}(h_i)$ and $\mathbf{E}(h_i)$ of the i th layer are observed. Until now, equations of PIM to obtain the correlation matrices \mathbf{F} , \mathbf{G} , \mathbf{Q} and \mathbf{E} are

available, and the algorithm is presented as below:

1. read the material properties and thickness h_i of the i th layer, wavenumber k , frequency ω .
2. calculate matrices \mathbf{A} , \mathbf{B} , \mathbf{C} and \mathbf{D} in Eq. (11); let $N_1=20$ and $N_2=20$, $\bar{h}_i = h_i/2^{N_1}$ and $\tau = \bar{h}_i/2^{N_2}$.
3. employ Eq. (30) to calculate $\mathbf{Q}(\tau)$, $\mathbf{G}(\tau)$, $\tilde{\mathbf{F}}(\tau)$ and $\tilde{\mathbf{E}}(\tau)$.

$\mathbf{Q}=\mathbf{Q}(\tau)$, $\mathbf{G}=\mathbf{G}(\tau)$, $\tilde{\mathbf{F}}=\tilde{\mathbf{F}}(\tau)$ and $\tilde{\mathbf{E}}=\tilde{\mathbf{E}}(\tau)$. Comment: initiation

4. for (iter=0; iter< N_2 ; iter++) Comment: PIM in the \bar{h}_i interval;

4.1 according to Eq. (35), compute \mathbf{Q}_c , \mathbf{G}_c , $\tilde{\mathbf{F}}_c$ and $\tilde{\mathbf{E}}_c$;

4.2 $\mathbf{Q}=\mathbf{Q}_c$, $\mathbf{G}=\mathbf{G}_c$, $\tilde{\mathbf{F}}=\tilde{\mathbf{F}}_c$ and $\tilde{\mathbf{E}}=\tilde{\mathbf{E}}_c$;

end $\rightarrow \mathbf{F}(\bar{h}_i)=\mathbf{I}+\tilde{\mathbf{F}}_c$, $\mathbf{E}(\bar{h}_i)=\mathbf{I}+\tilde{\mathbf{E}}_c$, $\mathbf{G}(\bar{h}_i)=\mathbf{G}_c$ and $\mathbf{Q}(\bar{h}_i)=\mathbf{Q}_c$. Comment: the correlation matrices $\mathbf{F}(\bar{h}_i)$, $\mathbf{G}(\bar{h}_i)$, $\mathbf{Q}(\bar{h}_i)$ and $\mathbf{E}(\bar{h}_i)$ of the given \bar{h}_i interval are obtained.

$\mathbf{F}_1=\mathbf{F}_2=\mathbf{F}(\bar{h}_i)$, $\mathbf{G}_1=\mathbf{G}_2=\mathbf{G}(\bar{h}_i)$, $\mathbf{Q}_1=\mathbf{Q}_2=\mathbf{Q}(\bar{h}_i)$ and $\mathbf{E}_1=\mathbf{E}_2=\mathbf{E}(\bar{h}_i)$. Comment: initiation

5. for (iter=0; iter< N_1 ; iter++) Comment: PIM in the h_i interval

5.1 use Eq. (27) to calculate \mathbf{F}_c , \mathbf{G}_c , \mathbf{Q}_c and \mathbf{E}_c ;

5.2 $\mathbf{F}_1=\mathbf{F}_2=\mathbf{F}_c$, $\mathbf{G}_1=\mathbf{G}_2=\mathbf{G}_c$, $\mathbf{Q}_1=\mathbf{Q}_2=\mathbf{Q}_c$ and $\mathbf{E}_1=\mathbf{E}_2=\mathbf{E}_c$;

end $\rightarrow \mathbf{F}(h_i)=\mathbf{F}_c$, $\mathbf{G}(h_i)=\mathbf{G}_c$, $\mathbf{Q}(h_i)=\mathbf{Q}_c$ and $\mathbf{E}(h_i)=\mathbf{E}_c$. Comment: the correlation matrices $\mathbf{F}(h_i)$, $\mathbf{G}(h_i)$, $\mathbf{Q}(h_i)$ and $\mathbf{E}(h_i)$ of the i th layer are achieved.

The combination of layers, which have different thickness and material properties, can be directly performed by Eq. (27). Consequently, one can obtain the following dual vector equation for the whole layered medium.

$$\bar{\mathbf{U}}_n = \mathbf{F}_N \bar{\mathbf{U}}_0 - \mathbf{G}_N \bar{\mathbf{S}}_n \quad \bar{\mathbf{S}}_0 = \mathbf{Q}_N \bar{\mathbf{U}}_0 + \mathbf{E}_N \bar{\mathbf{S}}_n \quad (36)$$

where the matrices \mathbf{F}_N , \mathbf{G}_N , \mathbf{Q}_N and \mathbf{E}_N are the correlation matrices from the surface layer to the n th layer; $\bar{\mathbf{U}}_0$ and $\bar{\mathbf{S}}_0$ are the displacement and stress at the free surface $z=0$; while $\bar{\mathbf{U}}_n$ and $\bar{\mathbf{S}}_n$ are the displacement and stress at the bottom surface $z=z_n$.

When the layered medium is placing on a rigid base, from the boundary condition $\bar{\mathbf{U}}_n=\mathbf{0}$ ($z=z_n$) and Eq. (36), the surface stress-displacement relation can be approached

$$\bar{\mathbf{U}}_0 = (\mathbf{Q}_N + \mathbf{E}_N \mathbf{G}_N^{-1} \mathbf{F}_N)^{-1} \bar{\mathbf{S}}_0 = \bar{\mathbf{G}}(k) \bar{\mathbf{S}}_0 \quad (37)$$

When the layered medium is resting on a semi-infinite space, from Eqs. (19) and (36), it obtains

$$\bar{\mathbf{U}}_0 = (\mathbf{Q}_N + \mathbf{E}_N \mathbf{R}_\infty (\mathbf{I} + \mathbf{G}_N \mathbf{R}_\infty)^{-1} \mathbf{F}_N)^{-1} \bar{\mathbf{S}}_0 = \bar{\mathbf{G}}(k) \bar{\mathbf{S}}_0 \quad (38)$$

where $\bar{\mathbf{G}}(k)$ represents the Green's function matrix in the wavenumber domain, which is expressed as

$$\begin{Bmatrix} \bar{u}_r(k) \\ \bar{u}_\theta(k) \\ \bar{u}_z(k) \end{Bmatrix} = \begin{bmatrix} \bar{G}_{rr}(k) & 0 & \bar{G}_{rz}(k) \\ 0 & \bar{G}_{\theta\theta} & 0 \\ \bar{G}_{zr}(k) & 0 & \bar{G}_{zz}(k) \end{bmatrix} \begin{Bmatrix} \bar{\tau}_{rz}(k) \\ \bar{\tau}_{\theta z}(k) \\ \bar{\sigma}_z(k) \end{Bmatrix} \quad (39)$$

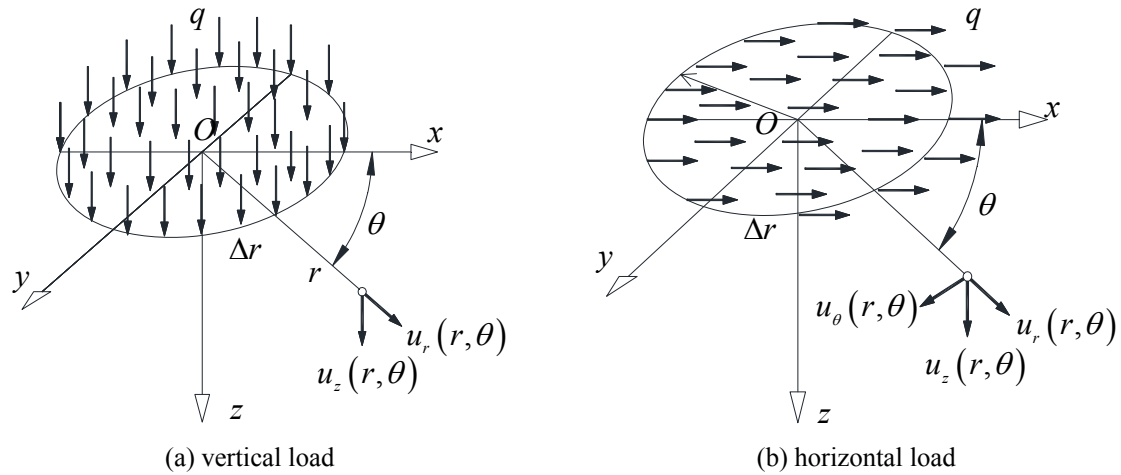


Fig. 2 Displacement under the uniformly distributed load on a disk

where element $\bar{G}_{ij}(k)$ ($i, j=r, \theta, z$) represents the flexibility coefficient in the wavenumber domain.

2.4 Green's function in the spatial domain

As mentioned before, similar domain transformations can be performed for the displacement vector \mathbf{U} as Eq. (2) via substituting the stress vector with the displacement vector. From Eqs. (2) and (39), the surface displacement due to the surface load in the spatial domain can be obtained

$$\mathbf{U}(r, \theta, z = 0) = \sum_{n=0}^{\infty} \mathbf{T}(n\theta) \int_{k=0}^{\infty} k \mathbf{C}_n(kr) \bar{\mathbf{G}}(k) \bar{\mathbf{S}}(k) dk \tag{40}$$

where $\bar{\mathbf{S}}(k)$ being the transform of the surface load in the wavenumber domain (Eq. (2)).

In the present study, the Green's function in the spatial domain is evaluated for the vertical and horizontal load conditions, which is the basis of the calculation of dynamic impedance functions. In the sequel, the calculations are associated within the ground $z=0$, for brevity, the term $z=0$ is dropped.

Considering a surface uniformly distributed vertical load q is acting on a disk of radius Δr , see Fig. 2(a). Using Eq. (2) to express the load in the wavenumber domain, at such load case $n=0$, it obtains

$$\bar{\sigma}_z(k) = \frac{1}{2\pi} \int_{r=0}^{\Delta r} r J_0(kr) \int_{\theta=0}^{2\pi} q d\theta dr = \frac{q\Delta r}{k} J_1(k\Delta r) \tag{41}$$

Substituting Eqs. (39) and (41) into (40), one can obtain the displacements in the spatial domain

$$\{u_r(r, \theta) \quad u_\theta(r, \theta) \quad u_z(r, \theta)\}^T = q\Delta r \int_{k=0}^{\infty} J_1(k\Delta r) [\bar{G}_{rz}(k) J_1(kr) \quad 0 \quad \bar{G}_{zz}(k) J_0(kr)]^T dk \tag{42}$$

The surface displacements, due to the surface uniformly distributed horizontal load (Fig. 2(b)), at such load case $n=1$, can be obtained similarly. For brevity, here we only present the final result

$$\begin{Bmatrix} u_r(r, \theta) \\ u_\theta(r, \theta) \\ u_z(r, \theta) \end{Bmatrix} = q\Delta r \begin{bmatrix} \cos\theta & 0 & 0 \\ 0 & -\sin\theta & 0 \\ 0 & 0 & \cos\theta \end{bmatrix} \left(\int_{k=0}^{\infty} \frac{1}{2} J_1(k\Delta r) \begin{bmatrix} 2J_1'(kr) & 2J_1(kr)/kr & 0 \\ 2J_1(kr)/kr & 2J_1'(kr) & 0 \\ 0 & 0 & -2J_1(kr) \end{bmatrix} \begin{Bmatrix} \bar{G}_{rr}(k) \\ \bar{G}_{\theta\theta}(k) \\ \bar{G}_{rz}(k) \end{Bmatrix} dk \right) \quad (43)$$

The Green's function for concentrated load can be obtained from those for disk load by considering the limit when Δr tends to zero. In the case of load with intensity F (horizontal or vertical load), the corresponding stress is $q=F/\pi\Delta r^2$. The limit expression for the displacement when $\Delta r \rightarrow 0$ are given below. The displacement due to the vertical concentrated load is

$$\{u_r(r, \theta) \quad u_\theta(r, \theta) \quad u_z(r, \theta)\}^T = \frac{F}{2\pi} \int_{k=0}^{\infty} k \left[\bar{G}_{rz}(k) J_1(kr) \quad 0 \quad \bar{G}_{zz}(k) J_0(kr) \right]^T dk \quad (44)$$

The displacement due to the horizontal concentrated load is

$$\begin{Bmatrix} u_r(r, \theta) \\ u_\theta(r, \theta) \\ u_z(r, \theta) \end{Bmatrix} = \frac{F}{\pi} \begin{bmatrix} \cos\theta & 0 & 0 \\ 0 & -\sin\theta & 0 \\ 0 & 0 & \cos\theta \end{bmatrix} \left(\int_{k=0}^{\infty} \frac{k}{4} \begin{bmatrix} 2J_1'(kr) & 2J_1(kr)/kr & 0 \\ 2J_1(kr)/kr & 2J_1'(kr) & 0 \\ 0 & 0 & -2J_1(kr) \end{bmatrix} \begin{Bmatrix} \bar{G}_{rr}(k) \\ \bar{G}_{\theta\theta}(k) \\ \bar{G}_{rz}(k) \end{Bmatrix} dk \right) \quad (45)$$

The surface force-displacement relation, obtained by Eqs. (42)-(45) in the local coordinate system, is transformed into the global cylindrical coordinate system as

$$\begin{Bmatrix} u_r(r, \theta) \\ u_\theta(r, \theta) \\ u_z(r, \theta) \end{Bmatrix} = \mathbf{G}\Gamma = \begin{bmatrix} G_{xr} & G_{yr} & G_{zr} \\ G_{x\theta} & G_{y\theta} & G_{z\theta} \\ G_{xz} & G_{yz} & G_{zz} \end{bmatrix} \begin{Bmatrix} \Gamma_x(x, y) \\ \Gamma_y(x, y) \\ \Gamma_z(x, y) \end{Bmatrix} \quad (46)$$

where Γ represents the resultant force of the applied load, $\Gamma=\pi\Delta r^2q$ (uniformly distributed load) and $\Gamma=F$ (concentrated load); (x, y) denotes the coordinate of the loading center; \mathbf{G} is the Green's function matrix; element G_{ij} ($i=x, y, z; j=r, \theta, z$) represents the flexibility coefficient, which indicates the displacement in the j direction at point (r, θ) when a unit load applied in the i direction at (x, y) .

2.5 Approach of numerical integration

To obtain the displacement in Eq. (40), infinite integrals involving Bessel functions should be performed numerically. Since Bessel functions are oscillation functions and tend to zero slowly with the increase of variable, common numerical integration methods, such as Simpson's rule or trapezoidal rule, are inadequate to achieve sufficient accuracy (Lucas 1995). However, the adaptive Gauss quadrature proposed by Chave (1983), Lucas (1995) are capable of executing these integrals. Thus, we adopt these approaches in the present study. Due to the difference of the integrands in the distributed and concentrated load case, the integrations should be performed separately. In the evaluation of displacement under concentrated load, such as Eqs. (44) and (45), only one Bessel function $J_m(kr)$ is involved in the integrands. The integrals can be executed by the method of Chave (1983). The details of the method can be approached in Chave (1983). Here, only the concept will be briefly introduced. To perform the infinite integrals involving one Bessel function, the integral is expressed as a finite sum of a sequence of partial integral terms.

$$H = \int_0^{\infty} f(k, z) J_m(kr) dk \approx \sum_{n=1}^N H_n = \sum_{n=1}^N \int_{k_n}^{k_{n+1}} f(k, z) J_m(kr) dk \quad (47)$$

in which k_n is the n th zero of $J_m(x)$ normalized by the range r .

Every partial integral terms H_n are then evaluated by the Gauss-Legendre quadrature method. It employs a combined relative-absolute error criterion to terminate the calculation. If the error criterion is not satisfied, new Gauss points are added. At each step, the integral kernel and Bessel function values are retained so that only the new integrand values need to be calculated. Summing the partial integrals leads to the complete integral. Due to the Bessel function's oscillatory behavior, it attains the convergence of the result slowly, also it may diverge if the integral kernel increases faster than $k^{1/2}$. To facilitate the calculation, in Chave (1983), it employs the continued fraction approach for the summation of the integral. We therefore adopt this algorithm. In the following analysis, the relative and absolute errors are set as 10^{-6} and 10^{-7} . It uses a three-point Gauss rule firstly with an extension to 7, 15, 31, 63, 127, and 255 common-point interlacing forms, which corresponds to integrating polynomials of degree 5, 11, 23, 47, 95, 191 and 383, respectively.

For the calculation of displacement under distributed load, such as Eqs. (42) and (43), the integrands involve products of Bessel functions of different orders, $J_m(kR)J_n(kr)$. Charve's method cannot be directly applied here. It has been studied by Lucas (1995) employing an adaptive Gauss quadrature. The detailed theoretical derivation of the method can be found in Lucas (1995). Still, we will briefly introduce the concept behind the method. The infinite integral of products of Bessel functions is expressed as a summation of two integrals

$$H = \int_0^\infty f(k, z) J_m(kR) J_n(kr) dk = \int_0^{k_{\max}} f(k, z) J_m(kR) J_n(kr) dk + \int_{k_{\max}}^\infty f(k, z) J_m(kR) J_n(kr) dk \quad (48)$$

where k_{\max} is the largest of the first zeros of $Y_m(kR)$ and $Y_n(kr)$; $Y_m(kR)$ and $Y_n(kr)$ are the Bessel functions of second kind. Both the finite and infinite integrals at the right-hand side in Eq. (48) are then evaluated by the adaptive Gaussian quadrature of Chave (1983). To facilitate the calculation, the ε -algorithm and mW transform are used to achieve high accuracy and efficiency.

3. Dynamic impedance functions of surface foundation

Fig. 1 illustrates an arbitrarily shaped rigid foundation on the surface of a multi-layered half space. In order to calculate the dynamic impedance functions, the soil-foundation interface is discretized into n sub square-elements (Fig. 1). The sum of the area of the sub square-elements equals to the total area of the foundation. In order to represent a traveling wave at a given frequency accurately, the maximum length of the sub square-elements should not be larger than $\Delta a \leq 2\pi c_s / 10\omega_{\max}$ (Jeremić *et al.* 2009). Here, ω_{\max} denotes the maximum excitation frequency; c_s represents the shear wave velocity of the surface layer, $c_s = \sqrt{\mu/\rho}$. A rigid foundation has three translational and three rotational degree-of-freedom as shown in Fig. 1. Assuming the harmonic responses at the foundation center are $(U_x, U_y, U_z)e^{i\omega t}$ and $(\Phi_x, \Phi_y, \Phi_z)e^{i\omega t}$ under steady-state loads $(F_x, F_y, F_z)e^{i\omega t}$ and $(M_x, M_y, M_z)e^{i\omega t}$. The loads are acting at the center of the foundation. The force-displacement relation with the corresponding amplitudes is as below, which is formulated in the degree-of-freedom of the foundation.

$$\mathbf{\Omega}_0(\omega) = \mathbf{S}(\omega)\mathbf{U}_0(\omega) \quad (49)$$

where $\mathbf{S}(\omega)$ represents the dynamic impedance functions of the foundation, which is a 6×6 matrix; $\mathbf{\Omega}_0(\omega)$ denotes generalized external force vector; $\mathbf{U}_0(\omega)$ represents generalized displacement vector

$$\mathbf{\Omega}_0 = \{F_x, F_y, F_z, M_x, M_y, M_z\}^T \quad \mathbf{U}_0 = \{U_x, U_y, U_z, \Phi_x, \Phi_y, \Phi_z\}^T \quad (50)$$

The dynamic impedance functions $\mathbf{S}(\omega)$ can be derived according to its definition: Fourier amplitude of the steady-state load exerts on the rigid foundation if a unit amplitude steady-state displacement occurs along any degree-of-freedom direction at a given frequency (Wolf 1985). To be specific, it is necessary to solve a mixed boundary-value problem: The vanishing tractions are imposed on the portion of the surface $z=0$, which is not covered by the rigid foundation. The displacement conditions, which are in the form of rigid-body displacements, are imposed on the contact areas of the foundation and soil. The surface force-displacement relation was obtained by Eq. (46) in the global coordinates. Employing Eq. (46), the force-displacement relation at the soil-foundation interface is

$$\mathbf{U}_\Gamma = \begin{Bmatrix} \mathbf{U}_\Gamma^1 \\ \mathbf{U}_\Gamma^2 \\ \vdots \\ \mathbf{U}_\Gamma^n \end{Bmatrix} = \begin{bmatrix} \mathbf{G}_u^{11} & \mathbf{G}_u^{12} & \cdots & \mathbf{G}_u^{1n} \\ \mathbf{G}_u^{21} & \mathbf{G}_u^{22} & \cdots & \mathbf{G}_u^{2n} \\ \vdots & \vdots & \ddots & \vdots \\ \mathbf{G}_u^{n1} & \mathbf{G}_u^{n2} & \cdots & \mathbf{G}_u^{nn} \end{bmatrix} \begin{Bmatrix} \mathbf{\Gamma}_0^1 \\ \mathbf{\Gamma}_0^2 \\ \vdots \\ \mathbf{\Gamma}_0^n \end{Bmatrix} = \mathbf{G}_u \mathbf{\Gamma}_0 \quad (51)$$

where $\mathbf{U}_\Gamma^i = [u_r^i \quad u_\theta^i \quad u_z^i]^T$ ($i=1,2,\dots,n$) denotes the average of the displacement over the i th sub-element in cylindrical coordinate system; $\mathbf{\Gamma}_0^j = [\Gamma_{x0}^j \quad \Gamma_{y0}^j \quad \Gamma_{z0}^j]^T$ ($j=1,2,\dots,n$) denotes the resultant of the tractions over the j th sub-element in Cartesian coordinate system, which is applied at the center of the j th sub-element; n corresponds to the number of sub-elements of the foundation. From Eq. (46), the Green's function matrix \mathbf{G}_u^{ij} ($i,j=1,2,\dots,n$) can be expressed

$$\mathbf{G}_u^{ij} = \begin{bmatrix} G_{xr}^{ij} & G_{yr}^{ij} & G_{zr}^{ij} \\ G_{x\theta}^{ij} & G_{y\theta}^{ij} & G_{z\theta}^{ij} \\ G_{xz}^{ij} & G_{yz}^{ij} & G_{zz}^{ij} \end{bmatrix} \quad (52)$$

where $G_{\alpha\beta}^{ij}$ ($\alpha=x,y,z; \beta=r,\theta,z$) represents the flexibility coefficient, which indicates the average of the displacement in the β direction at the i th sub-element when a unit concentrated load applied in the α direction at the center of the j th sub-element. Due to the singularity of the displacement at the loaded point (Kausel *et al.* 2000), the displacement within the loaded sub-element is evaluated by replacing the unit concentrated load via a uniformly distributed load $q=1/\pi\Delta r^2$ over a disk with radius $\Delta r = \Delta a/\sqrt{\pi}$, where Δa is the length of the sub square-element. Thus, we have two cases of evaluation of the Green's function matrix \mathbf{G}_u^{ij} ; for the concentrated load case, it can be calculated by Eqs. (44) and (45), and for the distributed load case, it can be obtained by Eqs. (42) and (43).

The displacement in the cylindrical coordinate system (Eq. (51)) should be transformed into the Cartesian coordinate system (Fig. 1) as below

$$\mathbf{U}_b = \begin{Bmatrix} \mathbf{U}_b^1 \\ \mathbf{U}_b^2 \\ \vdots \\ \mathbf{U}_b^n \end{Bmatrix} = \begin{bmatrix} \mathbf{H}_1 & 0 & \cdots & 0 \\ 0 & \mathbf{H}_2 & \cdots & 0 \\ \vdots & \vdots & \cdots & \vdots \\ 0 & 0 & \cdots & \mathbf{H}_n \end{bmatrix} \begin{bmatrix} \mathbf{G}_u^{11} & \mathbf{G}_u^{12} & \cdots & \mathbf{G}_u^{1n} \\ \mathbf{G}_u^{21} & \mathbf{G}_u^{22} & \cdots & \mathbf{G}_u^{2n} \\ \vdots & \vdots & \ddots & \vdots \\ \mathbf{G}_u^{n1} & \mathbf{G}_u^{n2} & \cdots & \mathbf{G}_u^{nn} \end{bmatrix} \begin{Bmatrix} \mathbf{\Gamma}_0^1 \\ \mathbf{\Gamma}_0^2 \\ \vdots \\ \mathbf{\Gamma}_0^n \end{Bmatrix} = \mathbf{\Pi} \mathbf{G}_u \mathbf{\Gamma}_0 \quad (53)$$

where $\mathbf{U}_b^i = [u_x^i \quad u_y^i \quad u_z^i]^T$ ($i=1,2,\dots,n$) denotes the average of the displacement over the i th sub-element in Cartesian coordinate system; the sub matrix \mathbf{H}_i ($i=1,2,\dots,n$) represents the transfer

matrix of the i th sub-element, which is defined as

$$\mathbf{H}_i = \begin{bmatrix} \cos \theta_i & -\sin \theta_i & 0 \\ \sin \theta_i & \cos \theta_i & 0 \\ 0 & 0 & 1 \end{bmatrix} \quad (54)$$

where θ_i is the circumferential angle of the i th sub-element, which can be obtained as

$$\cos \theta_i = x_i / \sqrt{x_i^2 + y_i^2} \quad \sin \theta_i = y_i / \sqrt{x_i^2 + y_i^2} \quad (55)$$

in which (x_i, y_i) is the coordinate of the center of the i th sub-element.

For the displacement boundary condition at the soil-foundation interface, the displacement field, averaged over each sub-element of the foundation, is given by $\mathbf{U}_b = \mathbf{A}\mathbf{U}_0$. \mathbf{U}_0 is defined in Eq. (50); \mathbf{A} denotes a $3n \times 6$ matrix connecting the motion of each sub-element with each of the rigid body degree-of-freedom of the foundation, which is given by

$$\mathbf{A} = \begin{bmatrix} 1 & 0 & 0 & 0 & 0 & -y_1 \\ 0 & 1 & 0 & 0 & 0 & x_1 \\ 0 & 0 & 1 & y_1 & -x_1 & 0 \\ \vdots & \vdots & \vdots & \vdots & \vdots & \vdots \\ 1 & 0 & 0 & 0 & 0 & -y_n \\ 0 & 1 & 0 & 0 & 0 & x_n \\ 0 & 0 & 1 & y_n & -x_n & 0 \end{bmatrix} \quad (56)$$

where (x_i, y_i) ($i=1,2,\dots,n$) is the coordinate of the centre of the i th sub-element.

Similarly, from the force equilibrium of the foundation, the generalized force $\mathbf{\Omega}_0$ in Eq. (50), exerted by the foundation on the soil, is given by $\mathbf{\Omega}_0 = \mathbf{A}^T \mathbf{\Gamma}_0$. $\mathbf{\Gamma}_0$ is the resultant forces over each of the sub-elements of the foundation (Eq. (53)).

Considering the displacement boundary condition and force equilibriums of the foundation, also incorporating Eq. (53) and comparing with Eq. (49), it obtains the dynamic impedance matrix $\mathbf{S}(\omega)$

$$\mathbf{S}(\omega) = \mathbf{A}^T \mathbf{G}_u^{-1} \mathbf{\Pi}^{-1} \mathbf{A} \quad (57)$$

The frequency domain solution for the dynamic impedance functions of surface foundation is function of foundation shape and dimension. In the most general case, the impedance functions $\mathbf{S}(\omega)$ is full and symmetric, i.e., all the rigid body motions of the foundation are interrelated. However, in the present study, the foundation rests on the surface of a horizontally layered half space. Also, the stress resultants act at the centre of the foundation. Thus, the torsional and vertical motions are completely decoupled from the remaining degree-of-freedoms. As a result, the matrix $\mathbf{S}(\omega)$ is

$$\mathbf{S}(\omega) = \begin{bmatrix} S_{11} & S_{12} & 0 & S_{14} & S_{15} & 0 \\ S_{12} & S_{22} & 0 & S_{24} & S_{25} & 0 \\ 0 & 0 & S_{33} & 0 & 0 & 0 \\ S_{14} & S_{24} & 0 & S_{44} & S_{45} & 0 \\ S_{15} & S_{25} & 0 & S_{45} & S_{55} & 0 \\ 0 & 0 & 0 & 0 & 0 & S_{66} \end{bmatrix} \quad (58)$$

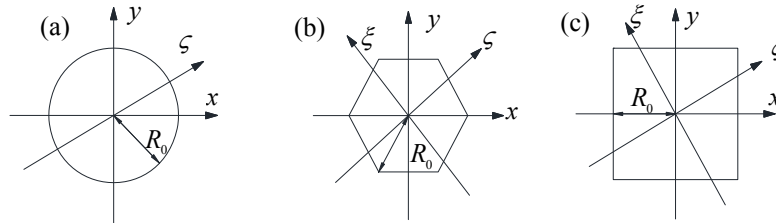


Fig. 3 Definition of axes for different geometries of foundation: (a) circular; (b) hexagonal; (c) square. The horizontal plane is considered, and all the foundations have the same characteristic length, R_0

where S_{ij} ($i, j=1, 2, \dots, 6$) denotes the impedance coefficient along the directions identified by the subscripts i and j (Fig. 1), which can be written as a uniform expression

$$S(a_0) = K_{st} (\bar{S}^r(a_0) + ia_0 \bar{S}^i(a_0)) \quad (59)$$

where K_{st} , $\bar{S}^r(a_0)$ and $\bar{S}^i(a_0)$ denote the static impedance coefficient, normalized spring constant and damping coefficient; $a_0 = \omega R/c_s$ and $c_s = \sqrt{\mu/\rho}$ denote the dimensionless frequency and the shear wave velocity of the surface layer; R is the characteristic length of the referred foundation, which could be defined as the radius of a circular foundation, or the half length of a square foundation of area equal to that of a rectangular foundation, or else as the radius of a circular foundation of area equal to the foundation of arbitrary shape.

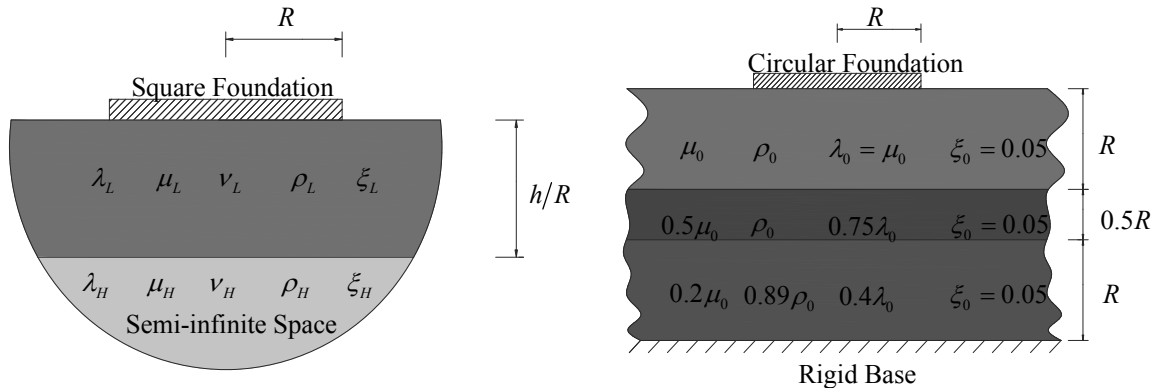
A further simplification of $\mathbf{S}(\omega)$ is performed if the moment of inertia around a given horizontal axis is invariant to a rotation of the foundation around the vertical axis. This is the case for the gravitation foundations that are typically utilized for wind turbines, i.e., circular, square and hexagonal foundation. With reference to Fig. 3, the moments of inertia are $I_x = I_y = I_\xi = I_\zeta$, where ζ is an arbitrary horizontal axis. As a result, $S_{11} = S_{22}$, $S_{44} = S_{55}$ and $S_{15} = -S_{24}$, and the coupling between the sliding in the x -direction and rocking in the y -direction (and vice versa) vanishes, i.e.

$$\mathbf{S}(\omega) = \begin{bmatrix} S_{11} & 0 & 0 & 0 & -S_{24} & 0 \\ 0 & S_{11} & 0 & S_{24} & 0 & 0 \\ 0 & 0 & S_{33} & 0 & 0 & 0 \\ 0 & S_{24} & 0 & S_{44} & 0 & 0 \\ -S_{24} & 0 & 0 & 0 & S_{44} & 0 \\ 0 & 0 & 0 & 0 & 0 & S_{66} \end{bmatrix} \quad (60)$$

Inverse of $\mathbf{S}(\omega)$ is the compliance matrix $\mathbf{C}(\omega)$, each element of compliance matrix can be written as

$$C(a_0) = C_{st} (\bar{C}^r(a_0) - i\bar{C}^i(a_0)) \quad (61)$$

where C_{st} , $\bar{C}^r(a_0)$ and $\bar{C}^i(a_0)$ denote the static compliance coefficient, the real and imaginary part of the compliance coefficient.



(a) Square foundation on a layered semi-infinite space (b) Circular foundation on a layered rigid base

Fig. 4 Foundation on a layered half space

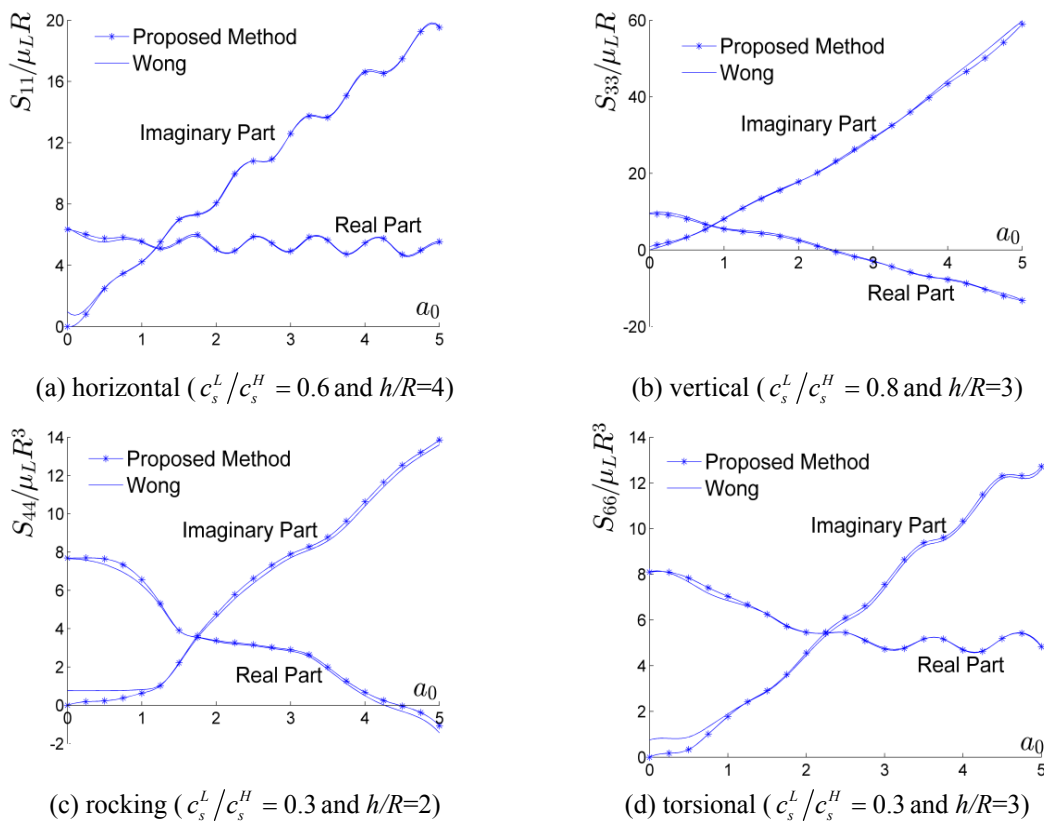


Fig. 5 Dynamic impedance coefficients for a rigid square foundation on a layered semi-infinite space

4. Applications: dynamic impedance of a rigid surface foundation

To validate the present solutions, three types of foundation are considered: rectangular, circular

and complex geometry. The first two cases are employed to validate the theory by comparing with the solutions in the literature, while the last one is presented to illustrate the capability of the proposed method for the analysis of a foundation with arbitrary shape. The soil-foundation interface is discretized into a number of sub square-elements. The length of the sub square-element Δa is obtained by $\Delta a \leq 2\pi c_s / 10\omega_{\max}$ (Jeremić *et al.* 2009). $c_s = \sqrt{\mu/\rho}$ denotes the shear wave velocity of the surface layer.

4.1 Dynamic impedance functions of a surface rectangular foundation

A surface square foundation of length $2R$ is considered; the soil medium consists of a layer overlying a semi-infinite space, see Fig. 4(a). The properties of the soil medium are: mass density $\rho_H = 1.13\rho_L$, Poisson's ratio $\nu_L = \nu_H = 0.45$, material damping ratio $\zeta_L = 0.05$ and $\zeta_H = 0.03$ and the ratio of the shear wave velocity c_s^L / c_s^H . The dimensionless frequency is defined as $a_0 = \omega R / c_s^L$. Wong has solved this problem by employing the transfer matrix method (Wong 1985). The evaluated impedance coefficients of the rigid rectangular foundation, normalized as given in Eq. (59), are shown in Fig. 5. Additionally, $\mu_L R$ and $\mu_L R^3$ are chosen as the dimensionless coefficients but not the static impedance coefficient K_{st} . After normalization, the real and imaginary part of the solution are depicted but not $\bar{S}^r(a_0)$ and $\bar{S}^i(a_0)$. The solution of Wong is denoted by solid line and is compared to the proposed approach (line with stars). Both curves coincide, which indicates that the proposed approach leads to correct results.

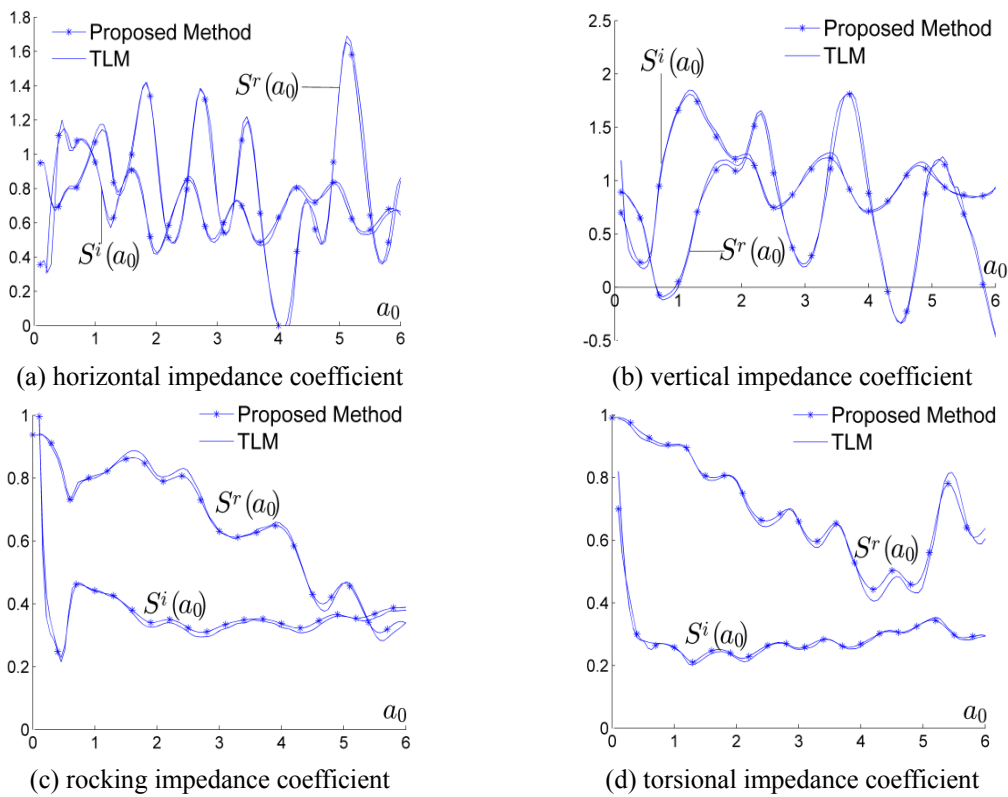


Fig. 6 Dynamic impedance functions of a circular foundation

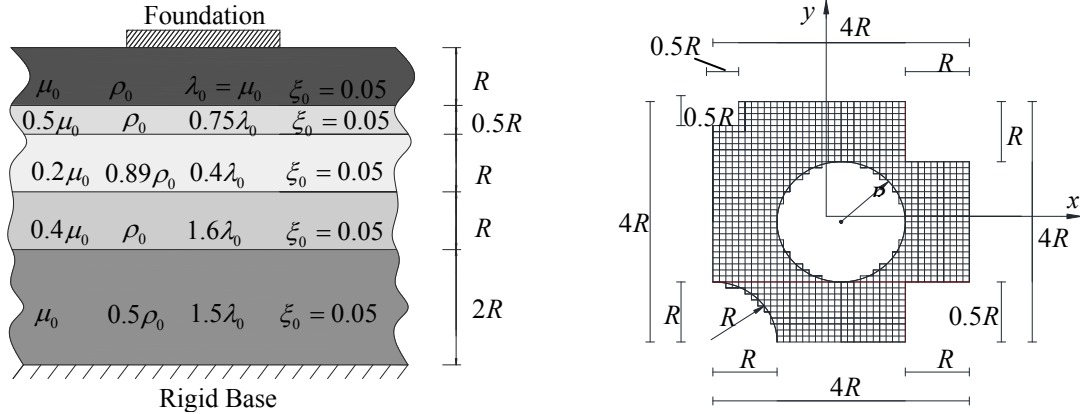


Fig. 7 Foundation with complex geometry on a five-layered rigid base

4.2 Dynamic impedance functions of a surface circular foundation

A surface circular foundation of radius R is considered; and the soil medium consists of three layers placed on a rigid base, see Fig. 4(b). Kausel (2003) has solved this problem by employing the thin layer method (TLM). The evaluated impedance coefficients of the rigid circular foundation, normalized as given in Eq. (59), are shown in Fig. 6. Here, K_{st} is selected as the static impedance coefficient of a rigid circular foundation placed on a homogeneous semi-infinite space which is with the material properties of the surface layer. K_{st} is equal to $8\mu_0R/(2-\nu_0)$, $4\mu_0R/(1-\nu_0)$, $8\mu_0R^3/(3(1-\nu_0))$ and $16\mu_0R^3/3$ for horizontal, vertical, rocking and torsional motion, respectively. $a_0 = \omega R/c_s$ and $c_s = \sqrt{\mu_0/\rho_0}$ denote the dimensionless frequency and the shear wave velocity of the surface layer. In the figure, the solution of TLM is denoted by solid line and is compared to the proposed approach (line with stars). It can be observed that the agreement among the two sets of results is fairly good, for the real part as well as for the imaginary part.

4.3 Dynamic impedance functions of a foundation with complex geometry

To illustrate the capability of the proposed method, the case of a rigid foundation with complex geometry in Fig. 7 is considered. The shape of the foundation is similar to that found in some real projects. In this example, the soil medium in Fig. 7 is employed here. The origin of the coordinate system is set at the center of the foundation. The impedance coefficients in Eq. (58) are shown in Fig. 8. Additionally, μ_0R and μ_0R^3 are chosen as the dimensionless coefficient but not the static impedance coefficient K_{st} . After normalization, the real and imaginary part of the solution are depicted but not $\bar{S}^r(a_0)$ and $\bar{S}^i(a_0)$. In order to show the effect of the supporting rigid base, the impedance of the foundation placed on a four layered semi-infinite space is also described in the figure. The four layered semi-infinite space includes the first four layers of the medium in Fig. 7 plus a semi-infinite space with the material properties of the fifth layer. The dimensionless frequency is defined as $a_0 = \omega R/c_s$, $c_s = \sqrt{\mu_0/\rho_0}$ denotes the shear wave velocity of the surface layer. In Fig. 8, the solid line denotes the impedance coefficients of foundation placed on the layered rigid base; while the line with stars demonstrates the impedance coefficients of foundation placed on the layered semi-infinite space. It can be observed that the impedance of layered rigid

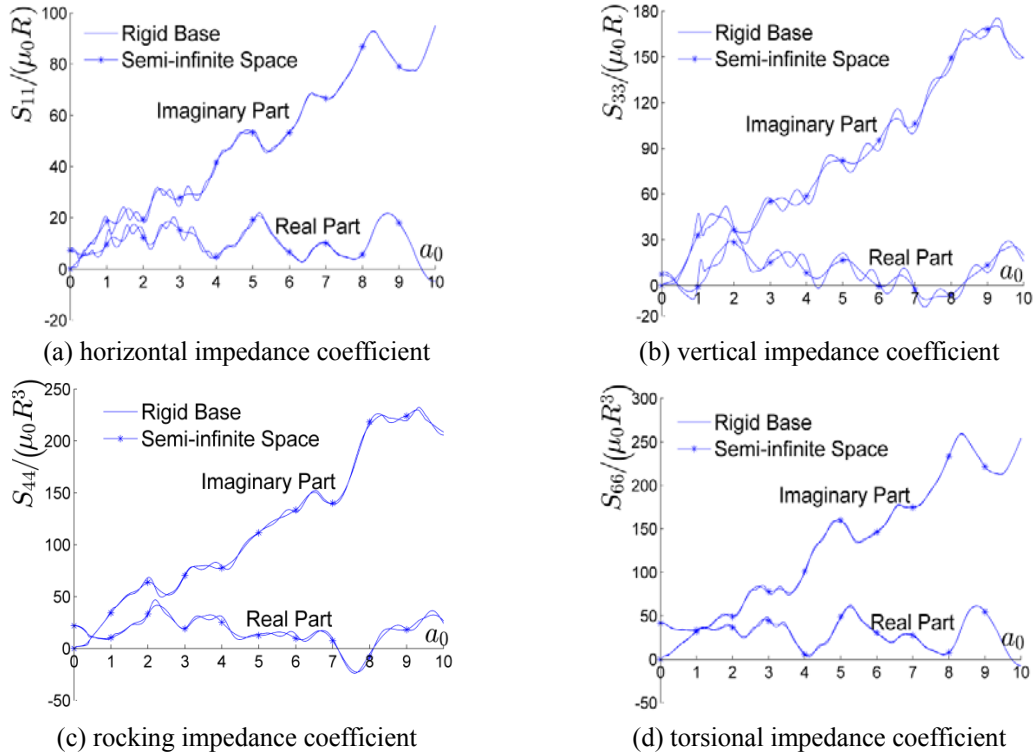


Fig. 8 Dynamic impedance functions of the foundation with complex geometry

base have a close resemblance to those of layered semi-infinite space in the range of large frequency a_0 ; and such resemblance is more remarkable in the cases of horizontal or torsional excitation than in the cases of vertical or rocking excitation.

5. Parameter study for the impedance and compliance functions

In the following, the effects of Poisson's ratio, material damping and contact condition of soil-foundation interface on the impedance and compliance functions are presented. The foundation considered here is a circular foundation of radius R placed on a homogeneous semi-infinite space with Poisson's ratio ν , shear modulus μ , material density ρ and material damping ratio ξ . The dimensionless frequency is defined as $a_0 = \omega R/c_s$. $c_s = \sqrt{\mu/\rho}$ denotes the shear wave velocity of the semi-infinite space. Here, for the horizontal, vertical, rocking and torsional motion of the circular foundation, the static impedance coefficients K_{st} in Eq. (59) equal to $8\mu R/(2-\nu)$, $4\mu R/(1-\nu)$, $8\mu R^3/(3(1-\nu))$ and $16\mu R^3/3$; and the static compliance coefficients C_{st} in Eq. (61) are $(2-\nu)/8\mu R$, $(1-\nu)/4\mu R$, $3(1-\nu)/8\mu R^3$ and $3/16\mu R^3$.

5.1 Material damping

The effect of material damping on the impedance functions is illustrated in Fig. 9. In the figure,

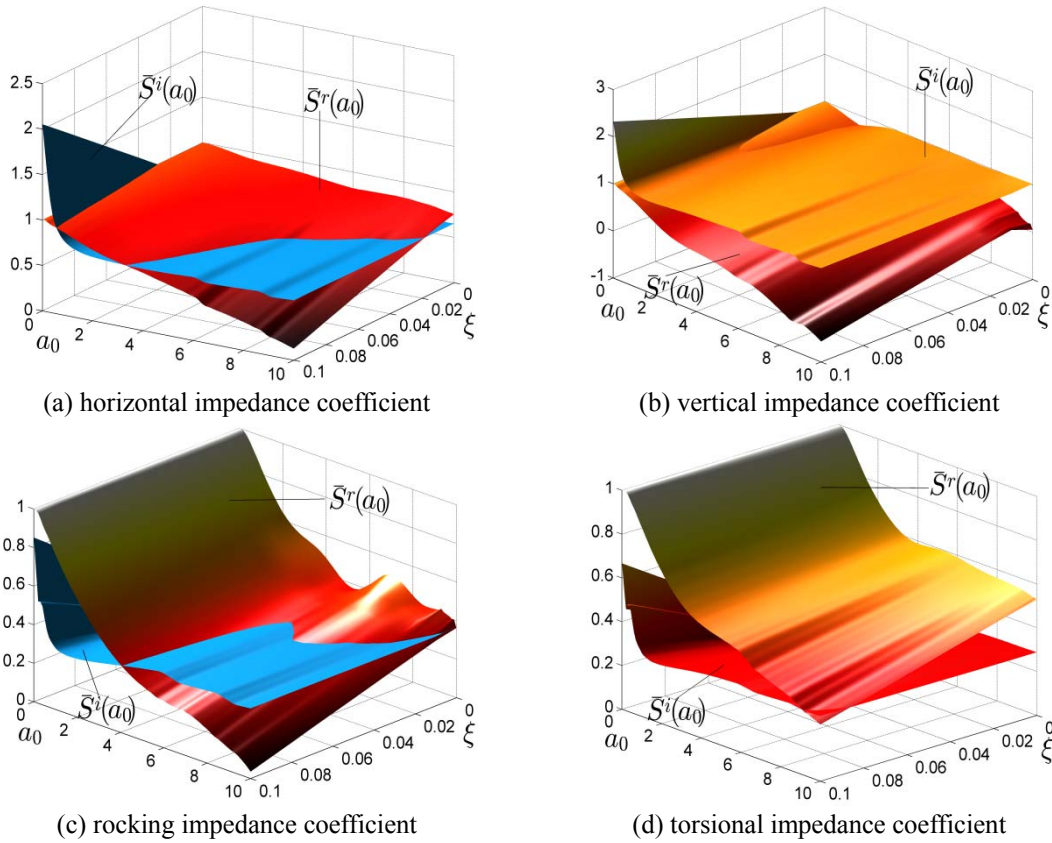


Fig. 9 Effect of material damping on the impedance functions ($\nu=0.3$)

the normalized spring constant and damping coefficient in Eq. (59) are shown for different values of material damping ratio. It can be observed that the material damping in the soil leads to a reduction in the normalized spring constant $\bar{S}^r(a_0)$ at higher frequencies while increases the damping coefficient $\bar{S}^i(a_0)$ at lower frequencies. Additionally, $\bar{S}^r(a_0)$ at lower frequencies and $\bar{S}^i(a_0)$ at higher frequencies tend to be constant. Kausel (1975) proposed an approximate approach for the dynamic impedance functions of a surface foundation on a viscoelastic semi-infinite space

$$S(a_0) = K_{st} (\bar{S}_r^*(a_0) + ia_0 \bar{S}_i^*(a_0)) (1 + 2\xi i) \tag{62}$$

where K_{st} , $\bar{S}_r^*(a_0)$ and $\bar{S}_i^*(a_0)$ denote the static impedance coefficient, the normalized spring constant and damping coefficient of the foundation placed on the same elastic semi-infinite space but without considering the material damping; ξ denotes the material damping ratio of the semi-infinite space. Expanding Eq. (62), one can obtain the following expression

$$S(a_0) = K_{st} (\bar{S}_r^*(a_0) - 2\xi a_0 \bar{S}_i^*(a_0) + ia_0 (\bar{S}_i^*(a_0) + \xi \bar{S}_r^*(a_0)/a_0)) \tag{63}$$

Comparing Eqs. (59) and (63), it can obtain

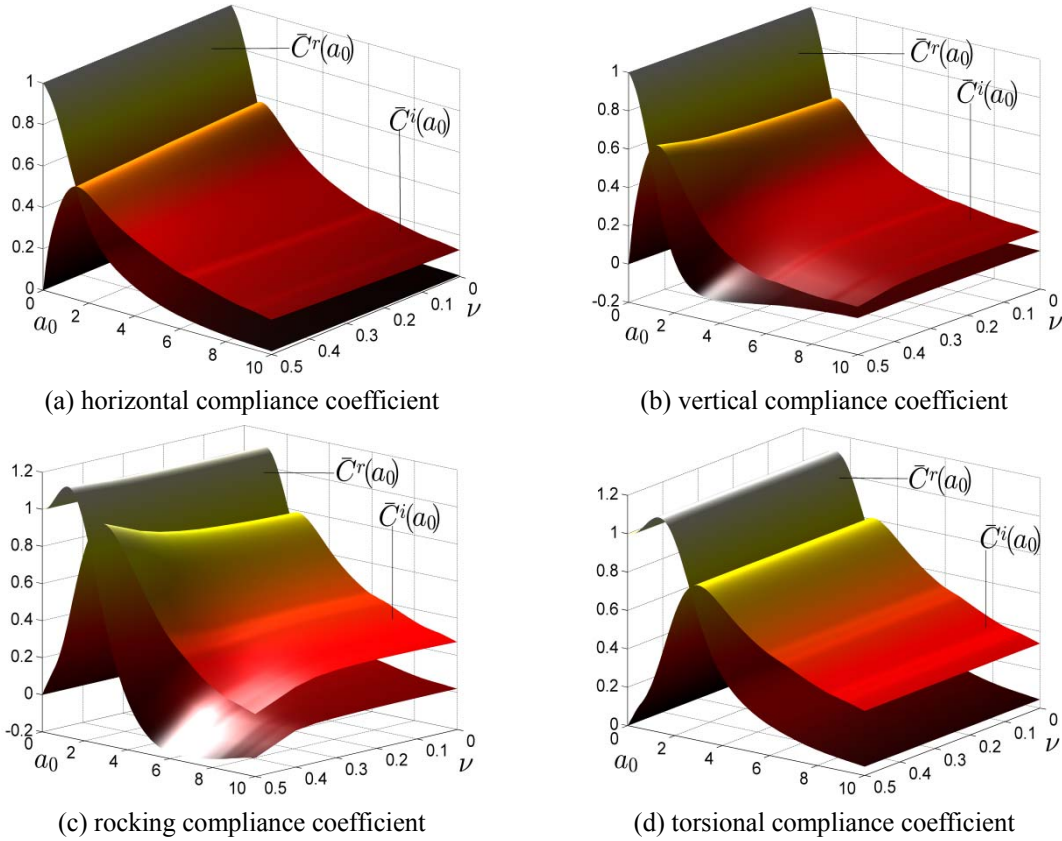


Fig. 10 Effect of Poisson’s ratio on the compliance functions ($\zeta=0.05$)

$$\bar{S}^r(a_0) = \bar{S}_r^*(a_0) - 2\xi a_0 \bar{S}_i^*(a_0) \quad \bar{S}^i(a_0) = \bar{S}_i^*(a_0) + \xi \bar{S}_r^*(a_0)/a_0 \quad (64)$$

Eq. (64) indicates that the normalized spring constant $\bar{S}^r(a_0)$ has negative relation with the material damping ratio and the damping coefficient $\bar{S}^i(a_0)$ has positive relation. At lower frequencies, the normalized spring constant changes little because the damping coefficient $\bar{S}_i^*(a_0)$ and the frequency a_0 are comparatively small. The same remark is suitable for the damping coefficient $\bar{S}^i(a_0)$ at higher frequencies due to the relatively small values of $\bar{S}_r^*(a_0)$ and large frequency a_0 . All these remarks are graphically proved by Fig. 9. In other words, the results of the proposed method validate the approximate formulas of Kausel (1975).

5.2 Poisson’s ratio

The Poisson’s ratio plays an important role on the compliance functions. The nature of this effect is illustrated in Fig. 10, in which the normalized compliance coefficients in Eq. (61) are presented. From the figures of horizontal compliance, it can be seen that the dynamic compliance does not depend much on Poisson’s ratio for lower values of frequencies and Poisson’s ratios, a fact already observed by Luco (1971). However, the Poisson’s ratio stresses more influence on the

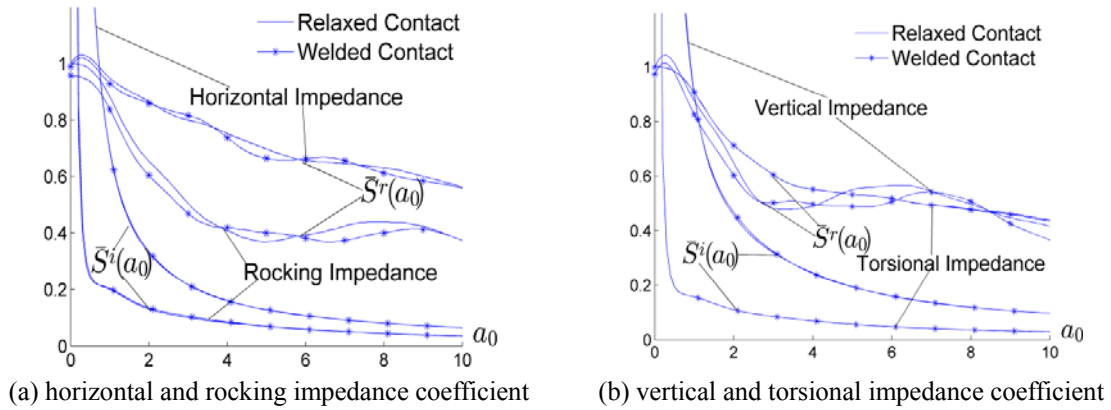


Fig. 11 Effect of contact condition on the impedance functions ($\nu=0.3, \zeta=0.05$)

vertical and rocking compliance: at lower frequencies, the real part of the compliance increases along with the Poisson's ratio; for higher frequencies and for Poisson's ratio close to one-half, the compliance coefficients reduce along with the Poisson's ratio; more importantly, the real part of the compliance becomes negative. For the torsional compliance, it can be observed that it does not change with the Poisson's ratio, which is consistent with the analytical solutions from Reissner and Sagoci (Reissner *et al.* 1944, Sagoci 1944). The interpretations are: the displacement, related to the forced torsional oscillations of the surface foundation, is the circumferential displacement u_θ ; and u_θ corresponds to the out-of-plane wave motion in the wavenumber domain; it involves only the shear modulus except Poisson's ratio in the solution of wave motion equation, see Eq. (5). Therefore, the torsional motion of the surface foundation is independent of the Poisson's ratio.

5.3 Contact condition

In general, a horizontal load will lead to both horizontal and vertical displacement, see Eq. (43). The same rule applies to the vertical load. Rigorously taking account of all components in \mathbf{G} of Eq. (46) leads to the dynamic impedance matrix $\mathbf{S}(\omega)$ for welded contact. As an approximation, only the diagonal terms in \mathbf{G} are considered, all the coupling terms are omitted. This represents the condition of relaxed contact. Under such contact condition, the coupled impedance coefficients are zero and the impedance matrix $\mathbf{S}(\omega)$ is a diagonal matrix; it is remarked that the calculation effort is reduced considerably. The influence of different contact conditions on the dynamic impedance functions is presented in Fig. 11. In the figure, the normalized spring constant and damping coefficient in Eq. (59) are shown. It represents the results of welded contact as line with stars and compares with the relaxed contact (solid line). It demonstrates very good agreement between the results of welded and relaxed contact is achieved; for the real part of the horizontal, vertical and rocking impedance some slight discrepancies exist, approximately 0~10% of the values of welded contact. Hence, in the practical applications, the off-diagonal terms in \mathbf{G} could be neglected to reduce the calculation effort.

It is worthwhile to note that the torsional impedance is identical for the two contact conditions. It can be illustrated like the influence of Poisson's ratio that: the displacement under the forced torsional oscillations of the foundation corresponds to the out-of-plane wave motion $\bar{u}_\theta(k)$ in the wavenumber domain. In Eq. (39), $\bar{u}_\theta(k)$ only relates to the flexibility coefficient $\bar{G}_{\theta\theta}$ without any

coupling terms. Hence, if it neglects the coupling terms, it will not influence the torsional motion of foundation.

6. Conclusions

A numerical procedure for the analysis of the forced vibration of a rigid surface foundation has been presented. It is based on domain-transformation, dual vector representation of wave motion equation and Precise Integration Method (PIM). Numerical results have been obtained for foundation not only with simple geometrical configurations, such as rectangular and circular, but also the case of irregularly shaped foundation. Comparison with the results of previous calculations in the literature has been made. Very good agreement is approached. A parametric study has been made on the dynamic response of the foundation. The effects of material damping, Poisson's ratio and contact condition of soil-foundation interface have been examined, which are illustrated as follows:

Material damping tends to reduce the normalized spring constant at higher frequencies. This trend begins at moderate frequencies and broadens as the frequency is increased. At lower frequencies, the material damping has negligible influence on the normalized spring constant; conversely, the effect on the damping coefficient are quite remarkable at lower frequencies, and the damping coefficient increases along with the material damping ratio. At higher frequencies, the material damping tends to have less influence on the damping coefficient.

From the analysis, the Poisson's ratio does not significantly affect the compliance functions at lower frequencies. It is more pronounced at higher frequencies and Poisson's ratio close to 0.5; the real part of the vertical and rocking compliance becomes negative. The torsional compliance does not depend on the Poisson's ratio.

Modifying the contact condition from welded to relaxed, it hardly affects any impedance functions, especially no influence on the torsional impedance. Thus, one can neglect the coupling terms to reduce the calculation effort in the practical applications.

References

- Abascal, R. and Dominguez, J. (1986), "Vibrations of footings on zoned viscoelastic soils", *J. Eng. Mech.*, **112**(5), 433-447.
- Alarcón, E., Cano, J.J. and Dominguez, J. (1989), "Boundary element approach to the dynamic stiffness functions of circular foundation", *Int. J. Numer. Anal. Methods Geomech.*, **13**(6), 645-664.
- Chave, A.D. (1983), "Numerical integration of related Hankel transforms by quadrature and continued fraction expansion", *Geophys.*, **48**(12), 1671-1686.
- Dominguez, J. and Roesset, J. (1978), "Dynamic stiffness of rectangular foundation", NASA STI/Recon Technical Report N 79, 16152.
- Ellis, E. and Springman, S. (2001), "Modelling of soil-structure interaction for a piled bridge abutment in plane strain FEM analyses", *Comput. Geotech.*, **28**(2), 79-98.
- Estorff, V.O. and Firuziaan, M. (2000), "Coupled BEM/FEM approach for nonlinear soil/structure interaction", *Eng. Anal. Bound. Elem.*, **24**(10), 715-725.
- Galvín, P., Romero, A. and Domínguez, J. (2010), "Fully three-dimensional analysis of high-speed train-track-soil-structure dynamic interaction", *J. Sound Vib.*, **329**(24), 5147-5163.
- Gao, Q., Lin, J.H., Zhong, W.X., Howson, W.P., Williams, F.W. (2006), "A precise numerical method for

- Rayleigh waves in a stratified half space”, *Int. J. Numer. Meth. Eng.*, **67**(6), 771-786.
- Gazetas, G. (1980), “Static and dynamic displacements of foundation on heterogeneous multilayered soils”, *Geotech.*, **30**(2), 159-177.
- Gazetas, G. (1981), “Strip foundation on a cross-anisotropic soil layer subjected to dynamic loading”, *Geotech.*, **31**(2), 161-179.
- Jeremić, B., Jie, G., Preisig, M. and Tafazzoli, N. (2009), “Time domain simulation of soil-foundation-structure interaction in non-uniform soils”, *Earthq. Eng. Struct. Dyn.*, **38**(5), 699-718.
- Ju, S.H., Ho, Y.S. and Leong, C.C. (2012), “A finite element method for analysis of vibration induced by maglev trains”, *J. Sound Vib.*, **331**(16), 3751-3761.
- Karabalis, D. and Beskos, D. (2006), “Dynamic response of 3-D rigid surface foundation by time domain boundary element method”, *Earthq. Eng. Struct. Dyn.*, **12**(1), 73-93.
- Karabalis, D.L. and Beskos, D.E. (1985), “Dynamic response of 3-D flexible foundation by time domain BEM and FEM”, *Int. J. Soil Dyn. Earthq. Eng.*, **4**(2), 91-101.
- Kausel, E. (1981), “An explicit solution for the Green’s function for dynamic loads in layered media”, NASA STI/Recon Technical Report N 82, 29505.
- Kausel, E. (2006), *Fundamental Solutions in Elastodynamics*, Cambridge University Press, Cambridge.
- Kausel, E. and Manolis, G.G.D. (2000), *Wave Motion Problems in Earthquake Engineering*, Wit Press.
- Kausel, E. and Roesset, J.M. (1975), “Dynamic stiffness of circular foundation”, *J. Eng. Mech. Div.*, **101**(6), 771-785.
- Kazakov, K.S. (2010), “Elastodynamic infinite elements with united shape functions for soil–structure interaction”, *Finite Elem. Anal. Des.*, **46**(10), 936-942.
- Kim, D.K. and Yun, C.B. (2003), “Time domain earthquake response analysis method for 2-D soil-structure interaction systems”, *Struct. Eng. Mech.*, **15**(6), 717-733.
- Lee, J.H. and Tassoulas, J.L. (2011), “Consistent transmitting boundary with continued-fraction absorbing boundary conditions for analysis of soil-structure interaction in a layered half-space”, *Comput. Meth. Appl. Mech. Eng.*, **200**(13), 1509-1525.
- Lehmann, L. (2005), “An effective finite element approach for soil-structure analysis in the time-domain”, *Struct. Eng. Mech.*, **21**(4), 437-450.
- Lin, G., Han, Z. and Li, J. (2013a), “An efficient approach for dynamic impedance of surface footing on layered half-space”, *Soil Dyn. Earthq. Eng.*, **49**, 39-51.
- Lin, G., Han, Z., Zhong, H. and Li, J. (2013b), “A precise integration approach for dynamic impedance of rigid strip footing on arbitrary anisotropic layered half-space”, *Soil Dyn. Earthq. Eng.*, **49**, 96-108.
- Lin, G., Han, Z. and Li, J. (2014), “Soil-structure interaction analysis on anisotropic stratified medium”, *Geotech.*, **64**(7), 570-580.
- Lucas, S. (1995), “Evaluating infinite integrals involving products of Bessel functions of arbitrary order”, *J. Comput. Appl. Math.*, **64**(3), 269-282.
- Luco, J. and Mita, A. (1987), “Response of a circular foundation on a uniform half-space to elastic waves”, *Earthq. Eng. Struct. Dyn.*, **15**(1), 105-118.
- Luco, J.E. (1975), “Impedance functions for a rigid foundation on a layered medium”, *Nucl. Eng. Des.*, **31**(2), 204-217.
- Luco, J.E. and Westmann, R.A. (1971), “Dynamic response of circular footings”, *J. Eng. Mech. Div.*, **97**(5), 1381-1395.
- Reissner, E. and Sagoci, H. (1944), “Forced torsional oscillations of an elastic half-space. I”, *J. Appl. Phys.*, **15**(9), 652-654.
- Rizos, D. and Wang, Z. (2002), “Coupled BEM-FEM solutions for direct time domain soil-structure interaction analysis”, *Eng. Anal. Bound. Elem.*, **26**(10), 877-888.
- Romero, A., Galvín, P. and Domínguez, J. (2013), “3D non-linear time domain FEM–BEM approach to soil–structure interaction problems”, *Eng. Anal. Bound. Elem.*, **37**(3), 501-512.
- Sagoci, H. (1944), “Forced torsional oscillations of an elastic half-space. II”, *J. Appl. Phys.*, **15**(9), 655-662.
- Said, I., De Gennaro, V. and Frank, R. (2009), “Axisymmetric finite element analysis of pile loading tests”, *Comput. Geotech.*, **36**(1), 6-19.

- Sheng, X., Jones, C.J.C. and Thompson, D.J. (2006), "Prediction of ground vibration from trains using the wavenumber finite and boundary element methods", *J. Sound Vib.*, **293**(3), 575-586.
- Spyrakos, C. and Beskos, D. (1986), "Dynamic response of rigid strip foundation by a time domain boundary element method", *Int. J. Numer. Meth. Eng.*, **23**(8), 1547-1565.
- Veletsos, A.S. and Verbič, B. (1973), "Vibration of viscoelastic foundation", *Earthq. Eng. Struct. Dyn.*, **2**(1), 87-102.
- Veletsos, A.S. and Wei, Y.T. (1971), "Lateral and rocking vibration of footings", *J. Soil Mech. Found. Div.*, **97**(9), 1227-1248
- Wolf, J.P. (1985), *Dynamic Soil-Structure Interaction*, Prentice-Hall.
- Wolf, J.P. and Preisig, M. (2003), "Dynamic stiffness of foundation embedded in layered halfspace based on wave propagation in cones", *Earthq. Eng. Struct. Dyn.*, **32**(7), 1075-1098.
- Wong, H. and Luco, J.E. (1985), "Tables of impedance functions for square foundation on layered media", *Int. J. Soil Dyn. Earthq. Eng.*, **4**(2), 64-81.
- Yalcin, O.F. and Mengi, Y. (2013), "A new boundary element formulation for wave load analysis", *Comput. Mech.*, **52**(4), 815-826.
- Zhang, J., Gao, Q., Tan, S.J. and Zhong, W.X. (2012), "A precise integration method for solving coupled vehicle-track dynamics with nonlinear wheel-rail contact", *J. Sound Vib.*, **331**(21), 4763-4773.
- Zhong, W.X. (2004), "On precise integration method", *J. Comput. Appl. Math.*, **163**(1), 59-78.
- Zhong, W.X. (2001), "Combined method for the solution of asymmetric Riccati differential equations", *Comput. Meth. Appl. Mech. Eng.*, **191**(1), 93-102.